Electronic Supplementary Material (ESI) for Journal of Materials Chemistry C.

Supplementary Information for

Solvent-free Mechanochemical Syntheses of Lead-free Hybrid Manganese Halides as Efficient Green light Phosphors

Yue-Yu Ma, [ab] *Ying-Rui Song,* [a] *Wen-Jie Xu,* [a] *Qian-Qian Zhong,* [a] *Han-Qi Fu,* [a] *Xue-Lei Liu,* [a] *Cheng-Yang Yue,* [a]* *Xiao-Wu Lei* [a]*

[a] Department of Chemistry and Chemical Engineering, Jining University, Qufu, Shandong, 273155, P. R. China

[b] College of Chemistry and Chemical Engineering, Qufu Normal University, Qufu, Shandong, 273165, P. R. China

Experimental Section

Table S2. The full and abbreviated name of organic salt used in this work.

Table S3. The ICP-OES results for all hybrid manganese halides.

Table S4. The elemental analysis results for all the hybrid manganese halides.

Table S5. The emission CIE of hybrid manganese halides and corresponding dominant wavelength as well as the color purity.

Table S6. Summary of the photophysical parameters of previously reported green-light emitting 0D manganese halides.

Table S7. Summary of the photophysical parameters of single crystalline lead halides and perovskite quantum dots or nanomaterials.

Table S8. Summary of the photophysical parameters of representative commercial inorganic green phosphors.

Table S9. Summary of photoluminescence parameters of 0D hybrid manganese halides prepared from wet-chemistry solution crystallization method.

Table S10. Summaries of the Mn···Mn distances and PLQYs of 0D hybrid manganese bromides obtained from wet-chemistry solution crystallization method.

Table S11-S13. Crystal data and structural refinements for 0D hybrid manganese halides.

Experimental Section

Materials

$MnBr_2 \cdot 4H_2O$ (99 %), $MnCl_2 \cdot 4H_2O$ (99 %), 1-ethyl-2,3-dimethylimidazolium bromide ([EMMIM]Br, 99%), 1-ethyl-2,3-dimethylimidazolium chloride ([EMMIM]Cl, 99%), 1-propyl-2,3-dimethylimidazolium bromide ([PMMIM]Br, 99%), tetramethylguanidine chloride ([TMGD]Cl, 99%s), tetrapropylammonium bromide ([TPA]Br, 98%,), tetrapropylammonium chloride ([TPA]Cl, 97%), 1-butyl-1-methylpiperidinium bromide ([BMPP]Br, 97%), 1-butylpyridinium bromide ([BPY]Br, 99%), benzyltriethylammonium bromide, ([BTEA]Br, 99%), 1-ethylpyridinium bromide ([EPY]Br, 99%), 1-ethyl-1-methylpyrrolidinium bromide, ([EMPR]Br, 99%), tetradecyltrimethylammonium bromide ([TTMA]Br, 99%), cetyltrimethylammonium bromide ([CTMA]Br, 99%), octadecyltrimethylammonium bromide ([OTMA]Br, 99%), 1,4-dimethylpiperazine ([DMPZ, 98%), ethanol (99%), 1-butanol (99%), 2-butanol (99%), isobutanol (99%), tert-butanol (99%), acetone (99%), hydrobromic acid (48%). Anhydrous $MnBr_2$ and $MnCl_2$ were obtained by vacuum heating $MnBr_2 \cdot 4H_2O$ and $MnCl_2 \cdot 4H_2O$ at 110°C for 12h, respectively. [DMPZ]Br_2 was prepared by the reaction of 1,4-dimethylpiperazine (5 mL) and HBr (5 mL) under sustained stir over 10 minutes and then rotary evaporation at 80°C.

Synthesis

Syntheses of microscale powders of hybrid manganese halides.

Precise control loading of mixture of organic salts and anhydrous MnX_2 according to fixed mole ratio was manually grinded using a mortar and pestle until the uniform slight green powder and steady green light intensity under UV light irradiation. The mole ratios of organic salts and MnX_2 was controlled to be 2 : 1 for all hybrid halides except 1 : 1 for [DMPZ]$MnBr_4$. The obtained microscale powder was dried under vacuum at 100°C for 1h to remove the absorbed crystal water in grinding process and then stored under vacuum.

Syntheses of bulk crystals of hybrid manganese halides

All the bulk single crystals of 0D hybrid manganese halides were prepared through wet-chemistry solution evaporation method at room temperature. Specifically, the mixtures of corresponding organic salt and manganese halides were dissolved in organic solvent, and the mixture was heated at 80°C under constant magnetic stirring for 10 minutes. The obtained solution was then cooled to room temperature and stayed for evaporation in atmosphere. After a few days, transparent crystals were obtained. The detailed preparation parameters are summarized in Table S1.

Table S1. Summarized preparation parameters of bulk crystals of title hybrid manganese halides.

	Organic salt	manganese halides	solution	yield
$[EMMIM]_2MnBr_4$	[EMMIM]Br (0.2 g)	$MnBr_2 \cdot 4H_2O$ (0.2 g)	ethanol (7 mL)	62%
$[BMPP]_2MnBr_4$	[BMPP]Br (0.2 g)	$MnBr_2 \cdot 4H_2O$ (0.2 g)	1-butanol (3 mL) acetone (2 mL)	62%
$[TPA]_2MnBr_4$	[TPA]Br (0.2 g)	$MnBr_2 \cdot 4H_2O$ (0.2 g)	ethanol (7 mL)	59%
$[TMGD]_2MnCl_4$	[TMGD]Cl (0.15 g)	$MnCl_2 \cdot 4H_2O$ (0.15 g)	ethanol (7 mL)	55%
$[PMMIM]_2MnBr_4$	[PMMIM]Br (0.2 g)	$MnBr_2 \cdot 4H_2O$ (0.2 g)	ethanol (3 mL) isobutanol (2 mL)	78%
$[EMMIM]_2MnCl_4$	[EMMIM]Cl (0.15 g)	$MnCl_2 \cdot 4H_2O$ (0.15 g)	1-butanol (5 mL)	57%
$[BPY]_2MnBr_4$	[BPY]Br (0.2 g)	$MnBr_2 \cdot 4H_2O$ (0.2 g)	acetone (5 mL)	61%
$[BMPR]_2MnBr_4$:	[BMPR]Br (0.2 g)	$MnBr_2 \cdot 4H_2O$ (0.2 g)	acetone (5 mL) 1-butanol (1 mL)	51%
$[BTEA]_2MnBr_4$	[BTEA]Br (0.2 g)	$MnBr_2 \cdot 4H_2O$ (0.2 g)	ethanol (5 mL)	83%
$[TPA]_2MnCl_4$	[TPA]Cl (0.2 g)	$MnCl_2 \cdot 4H_2O$ (0.15 g)	ethanol (3 mL) tertbutanol (2 mL)	44%
$[EPY]_2MnBr_4$	[EPY]Br (0.2 g)	$MnBr_2 \cdot 4H_2O$ (0.15 g)	ethanol (5 mL)	49%

[DMPZ]$MnBr_4$	[DMPZ] (0.1 g)	$MnBr_2 \cdot 4H_2O$ (0.15 g)	ethanol (5 mL) HBr (1 mL)	43%
$[EMPR]_2MnBr_4$	[EMPR]Br (0.15 g)	$MnBr_2 \cdot 4H_2O$ (0.1 g)	ethanol (5 mL)	7.5%

Physicochemical characterizations

Powder X-ray diffraction (PXRD) data were measured on a Bruker D8 ADVANCE powder X-ray diffractometer (Cu Kα, λ=1.5418 Å) in the 2θ range of 5–60°. UV-Vis absorption spectrum was monitored with a PE Lambda 900 UV/vis spectrophotometer in the wavelength range of 200–800 nm. The IR spectra were measured on a Thermo Fisher Nicolet iS5 FT-IR spectrograph in the wavelength range of 400-4000 cm^{-1}. The thermal behavior (TGA) was implemented on a Mettler TGA/SDTA 851 thermal analyzer under a N_2 atmosphere with a heating rate of 10°C/min^{-1} from 25°C to 800 °C. Scanning electron microscopy (SEM) images were obtained by a Zeiss Sigma 500. The excitation spectrum was measured at room temperature on an Edinburgh FLS980 fluorescence spectrometer in wavelength range of 250–500 nm at maximum of emission spectra. The emission spectrum was measured at room temperature on an Edinburgh FLS980 fluorescence spectrometer in wavelength range of 450-650 nm at maximum of excitation spectra. The power-dependent PL spectra were measured using the 375 nm (LE-LS-375-140TFCA, 1–140 mW). The absolute quantum yield was acquired using an integrating sphere incorporated into the FLS980 fluorescence spectrometer with a Xe lamb. The PLQY was calculated by the equation: $\eta_{QY} = I_S/(E_R - E_S)$, in which I_S represents the luminescence emission spectrum of the sample, E_R is the spectrum of the excitation light from the empty integrated sphere (without the sample), and E_S is the excitation spectrum for exciting the sample. Time-Resolved Emission data were collected at room temperature using the FLS980 fluorescence spectrometer. The dynamics of emission decay were monitored by using the FLS980's time-correlated single-photon counting capability (1024 channels; 1 μs window) with data collection for 10,000 counts. Excitation was provided by an

Edinburgh EPL-360 picosecond pulsed diode laser. The CIE calculator software was used to calculate the CIE chromaticity coordinates based on the emission spectra.

Crystallographic Studies

All the single crystal data of title compounds were collected on Bruker X-ray diffractometer (SMART II, Mo-K_α, λ= 0.71073 Å) at 296 K. The single crystal data were directly solved and refined based on F^2 by using SHELXTL-97 software. All the C, N, Mn, Cl and Br atoms were refined with anisotropic thermal vibration factors except the H atoms, which were theoretically defined according to geometrical configurations of organic groups and refined with isotropic thermal vibration factors. Important structural refinement parameters are summarized in Table S8-10 in the Supporting Information and crystallographic data are also supplied.

Fabrication of White LED Lamp

The UV pumped white LED device was fabricated by combining a 365 nm UV LED chip with the green phosphor of hybrid manganese halides, red phosphor of $K_2SiF_6:Mn^{4+}$ and blue phosphor of $BaMgAl_{10}O_{17}:Eu^{2+}$. Firstly, the sample and phosphor are mixed and ground with glue for 10 minutes. Then the mixtures were degassed in a vacuum oven for 5 minutes at room temperature. Finally, the mixtures were coated on the surface of the UV chip, and cured for 30 minutes. The EL properties of the fabricated white LED were evaluated by a high accuracy spectroradiometer (Everfine, HAAS-2000) with an integrating sphere (Everfine, ATA-500). The as-fabricated white LED were operated at 3 V in various drive currents from 20 to 120 mA.

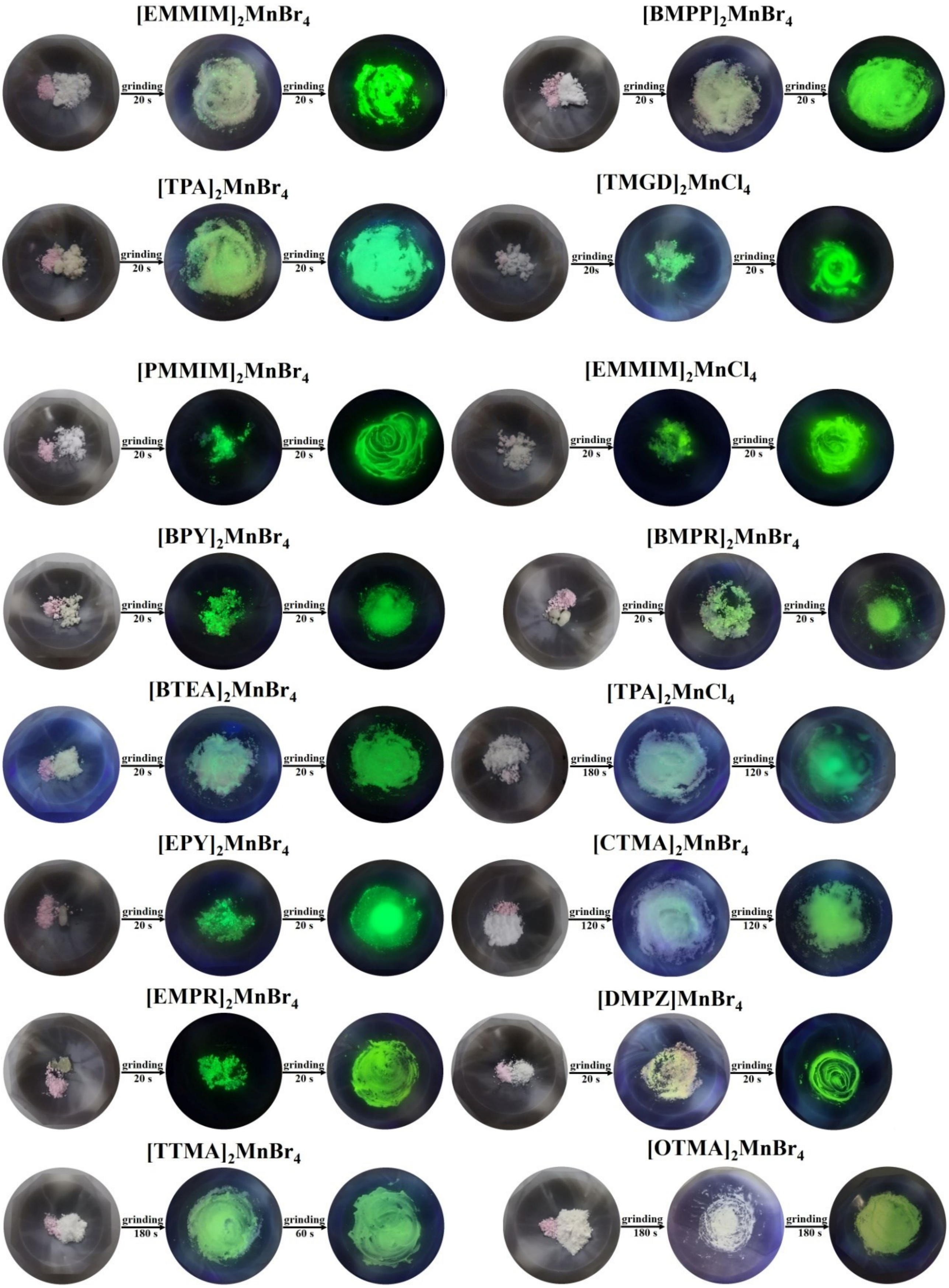

Fig. S1. The mechanical grinding preparation processes of microscale hybrid manganese halides.

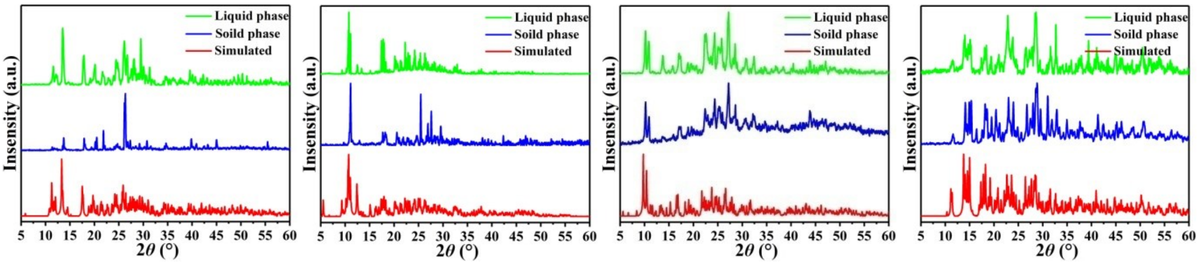

[EMMIM]$_2$MnBr$_4$ (**1**) [BMPP]$_2$MnBr$_4$ (**2**) [TPA]$_2$MnBr$_4$ (**3**) [TMGD]$_2$MnCl$_4$ (**4**)

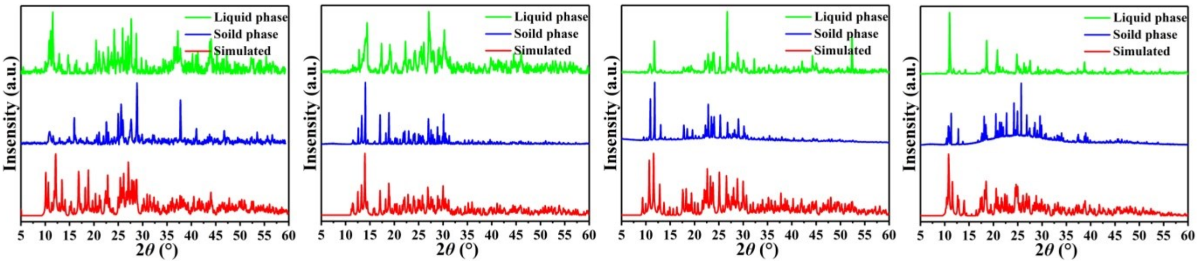

[PMMIM]$_2$MnBr$_4$ (**5**) [EMMIM]$_2$MnCl$_4$ (**6**) [BPY]$_2$MnBr$_4$ (**7**) [BMPR]$_2$MnBr$_4$ (**8**)

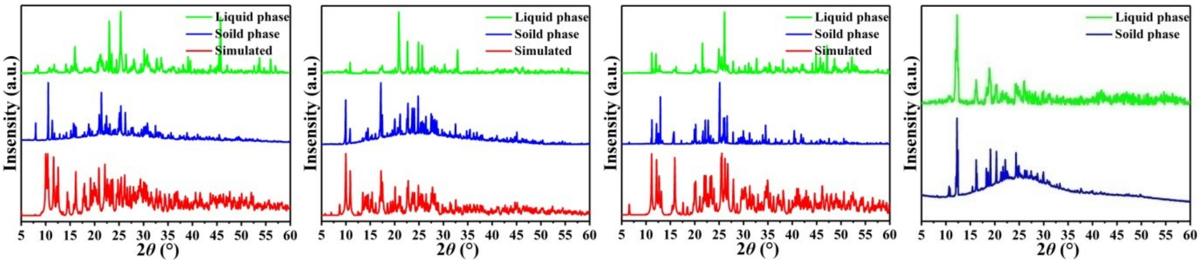

[BTEA]$_2$MnBr$_4$ (**9**) [TPA]$_2$MnCl$_4$ (**10**) [EPY]$_2$MnBr$_4$ (**11**) [EMPR]$_2$MnBr$_4$ (**13**)

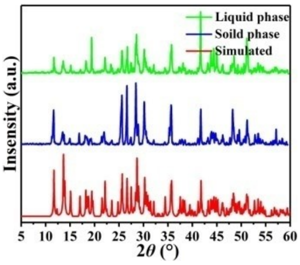

[DMPZ]MnBr$_4$ (**14**)

Fig. S2. The simulated and experimental PXRD patterns of microscale and bulk crystals for hybrid manganese halides prepared form mechanical grinding solid-state reaction and solution crystallization method, respectively.

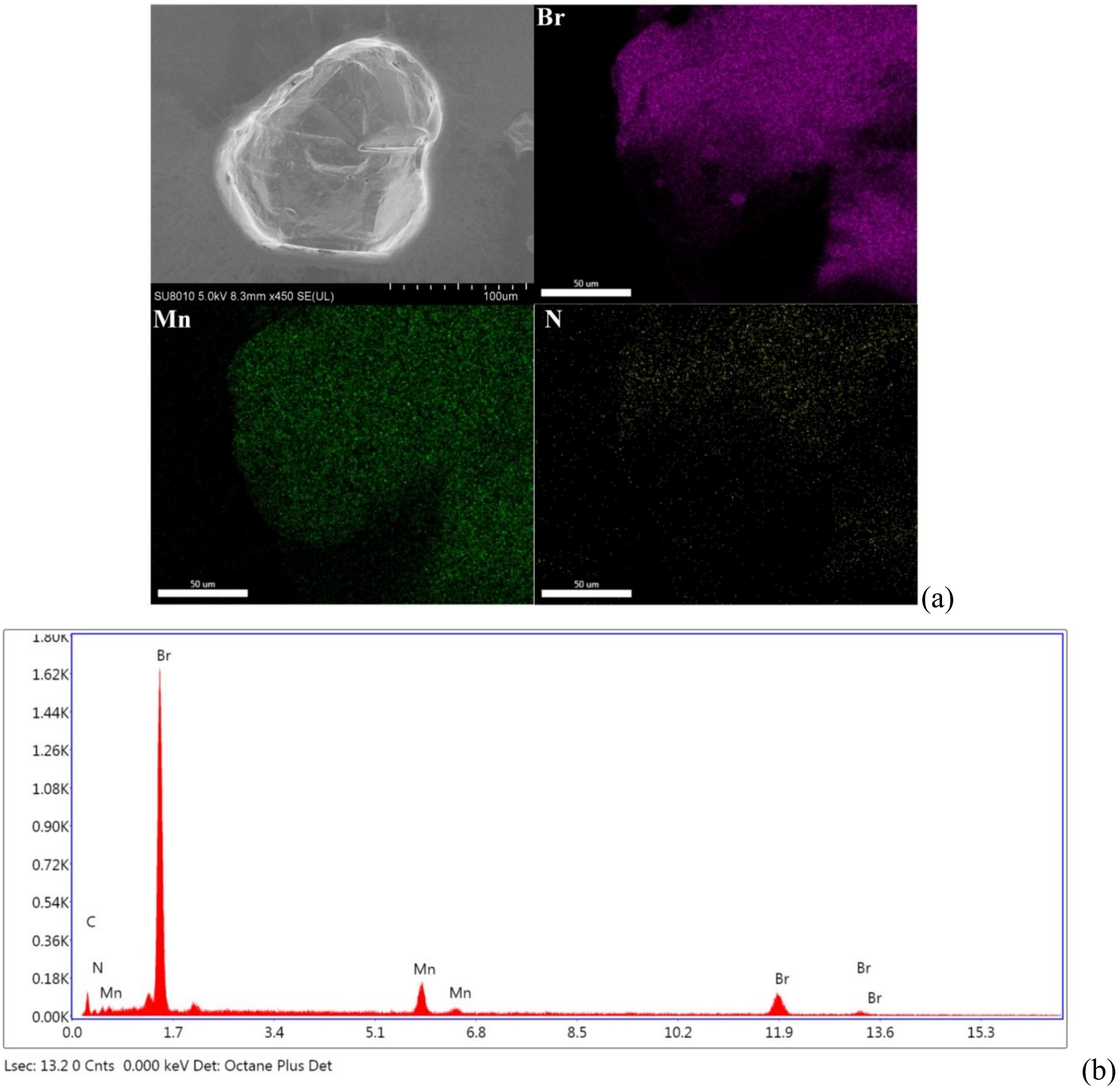

Fig. S3. The SEM image (a) and EDX analysis result (b) of microscale $[EMMIM]_2MnBr_4$ (**1**) prepared form mechanical grinding solid-state reaction.

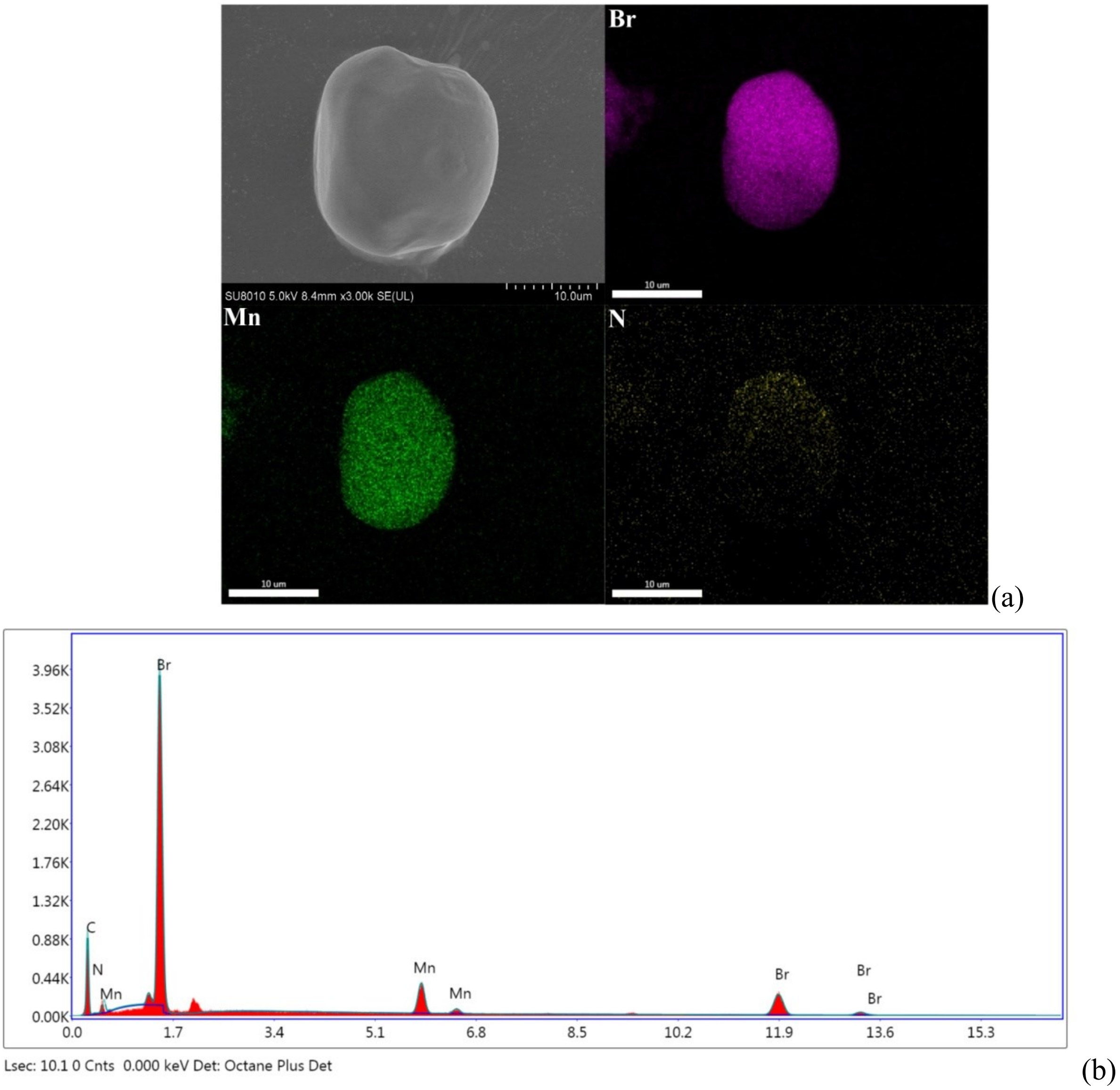

Fig. S4. The SEM image (a) and EDX analysis result (b) of microscale $[BuMPP]_2MnBr_4$ (**2**) prepared form mechanical grinding solid-state reaction.

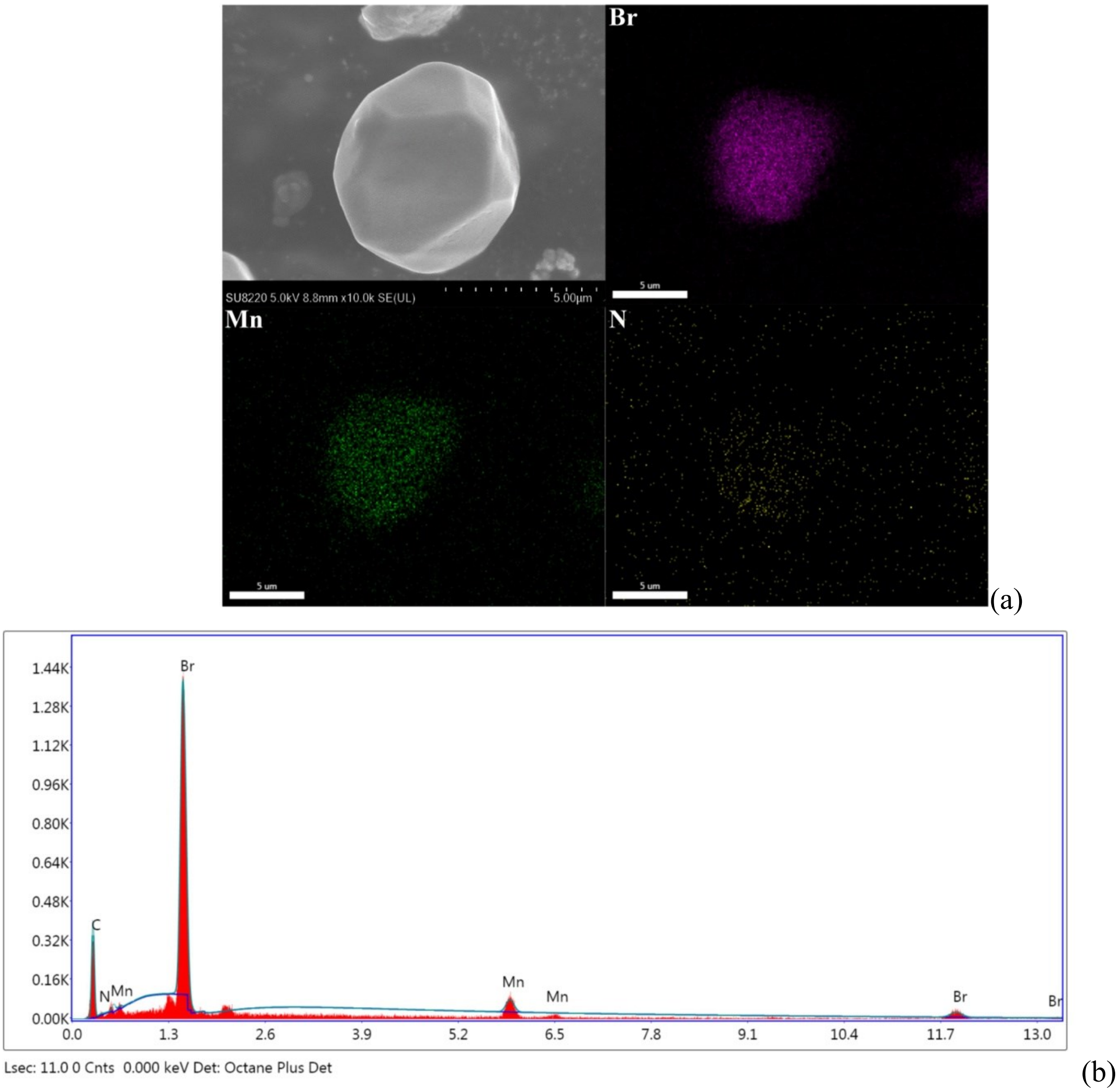

Fig. S5. The SEM image (a) and EDX analysis result (b) of microscale $[TPA]_2MnBr_4$ (**3**) prepared form mechanical grinding solid-state reaction.

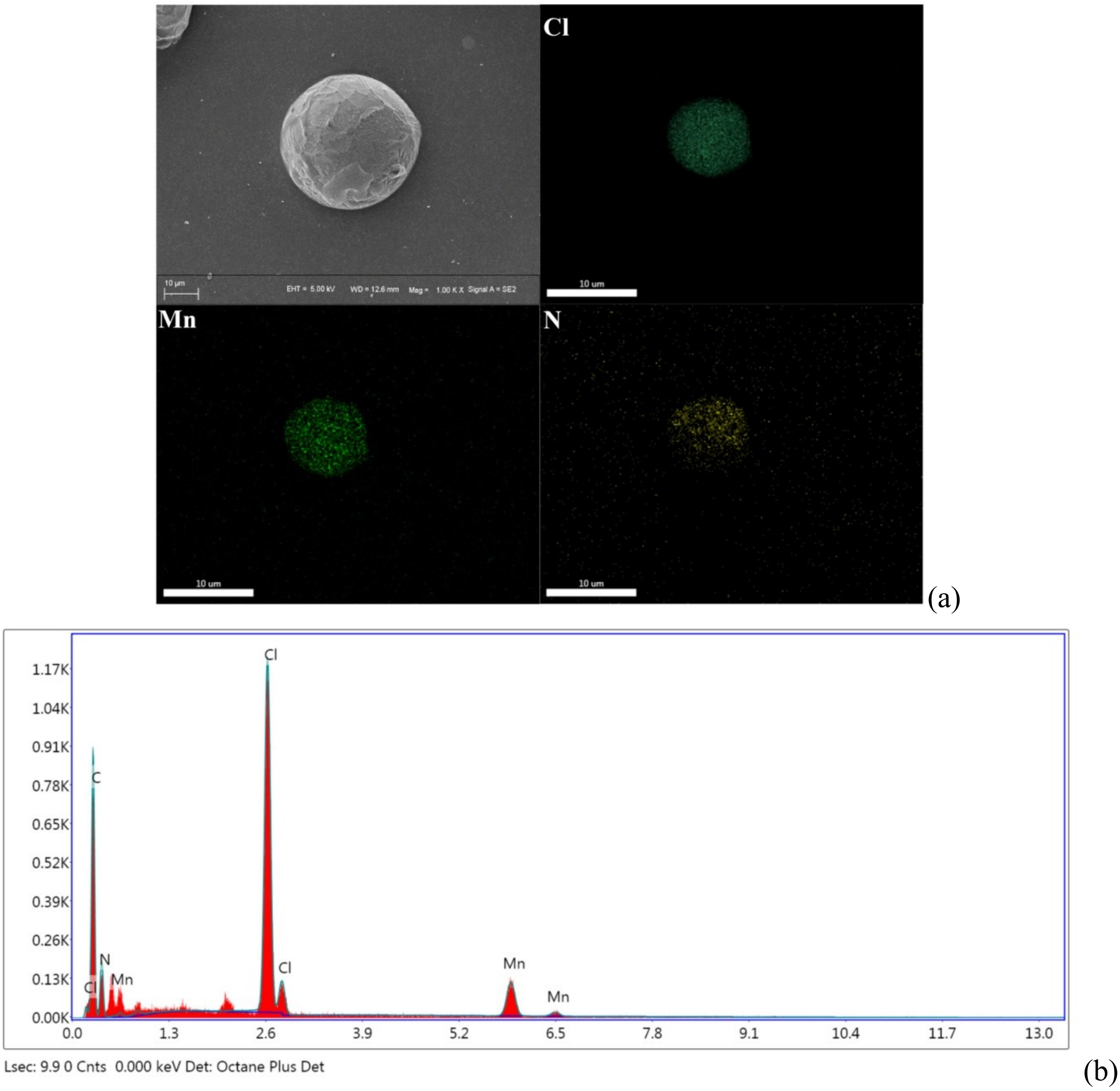

Fig. S6. The SEM image (a) and EDX analysis result (b) of microscale $[TMGD]_2MnCl_4$ (**4**) prepared form mechanical grinding solid-state reaction.

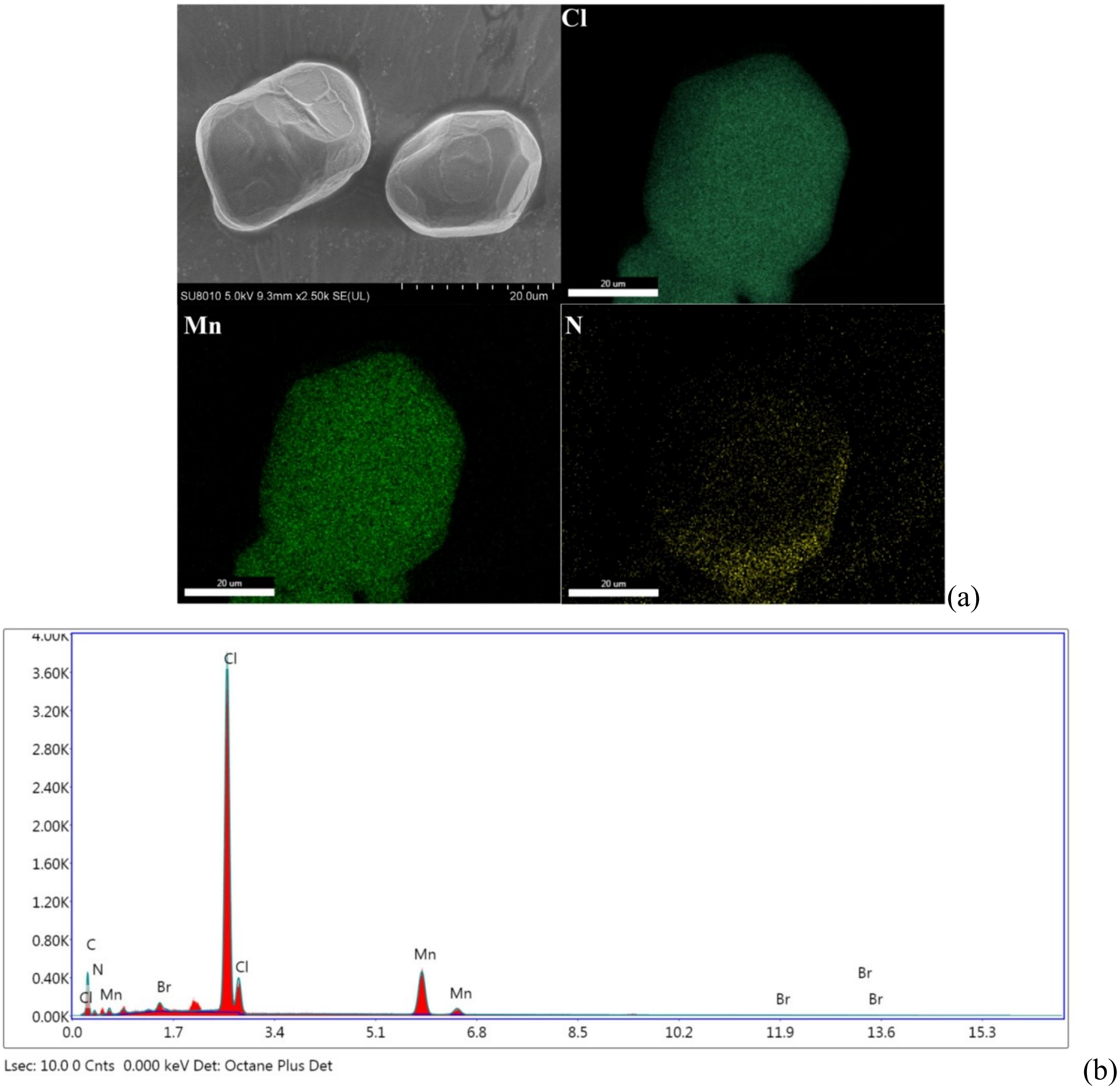

Fig. S7. The SEM image (a) and EDX analysis result (b) of microscale $[EMMIM]_2MnCl_4$ (**6**) prepared form mechanical grinding solid-state reaction.

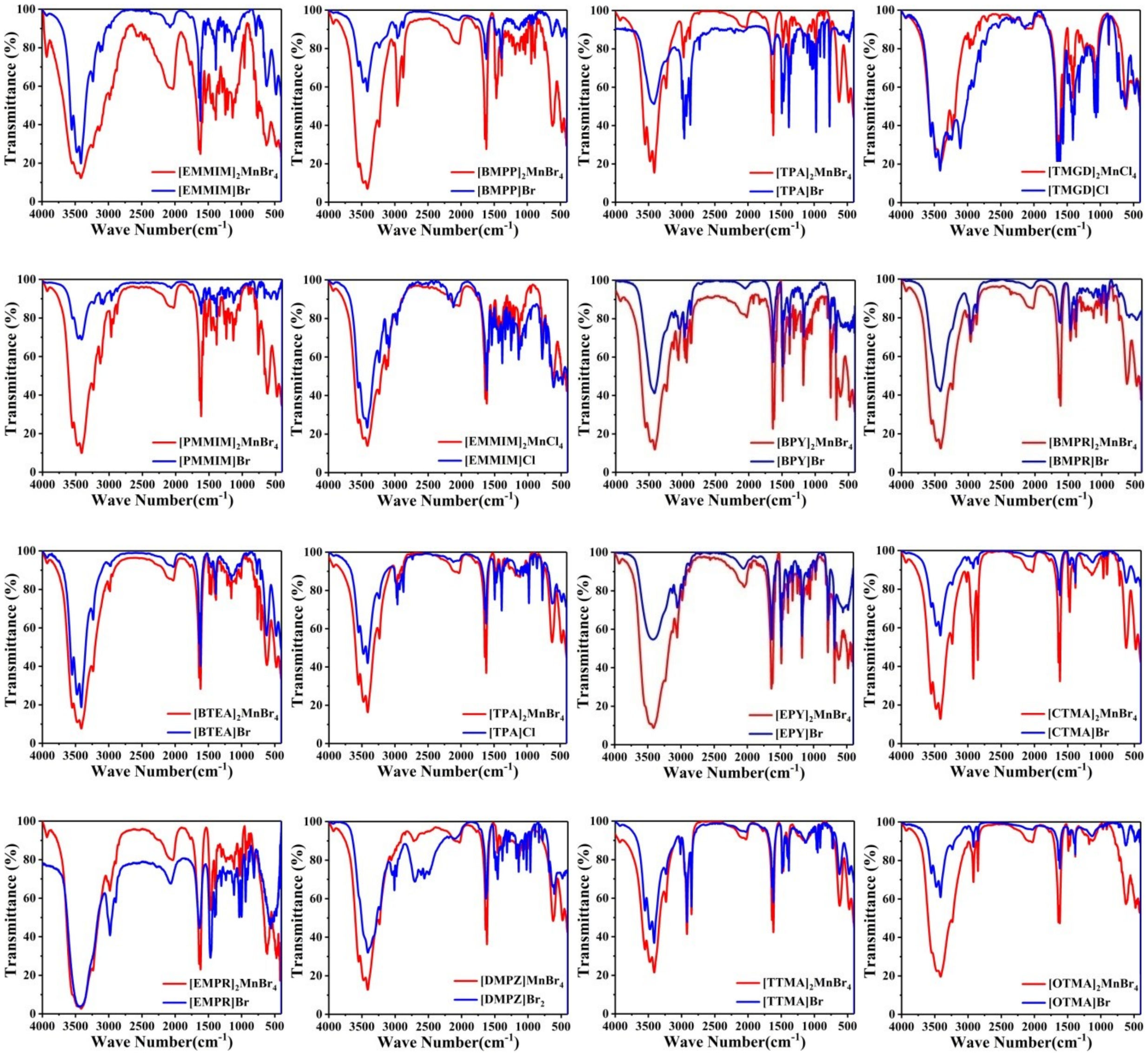

Fig. S8. Comparisons of the infra-red spectra of microscale hybrid manganese halides prepared from mechanical grinding solid-state reaction and precursor organic salts.

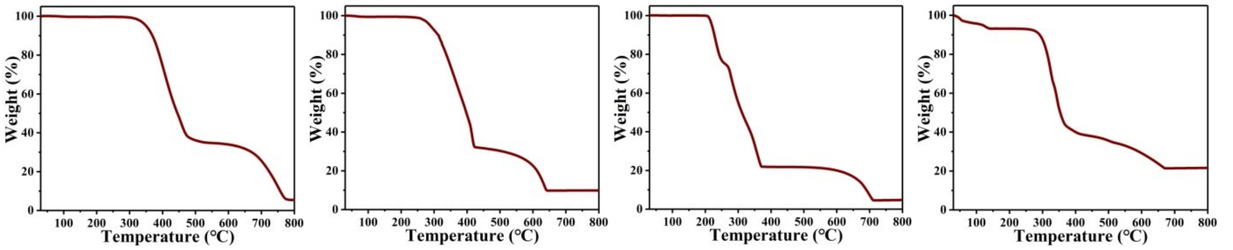

[EMMIM]$_2$MnBr$_4$ (**1**) [BMPP]$_2$MnBr$_4$ (**2**) [TPA]$_2$MnBr$_4$ (**3**) [TMGD]$_2$MnCl$_4$ (**4**)

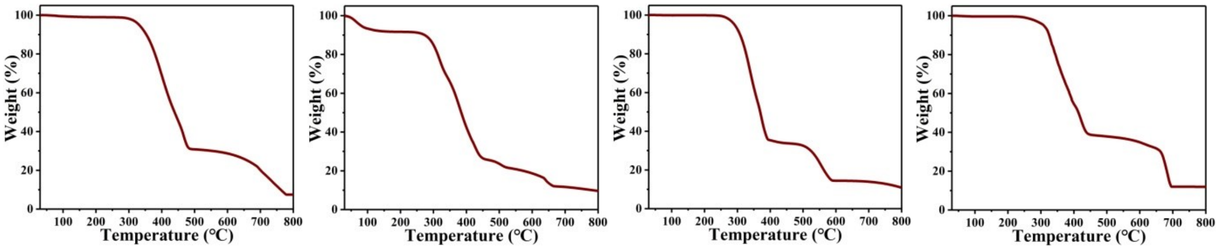

[PMMIM]$_2$MnBr$_4$ (**5**) [EMMIM]$_2$MnCl$_4$ (**6**) [BPY]$_2$MnBr$_4$ (**7**) [BMPR]$_2$MnBr$_4$ (**8**)

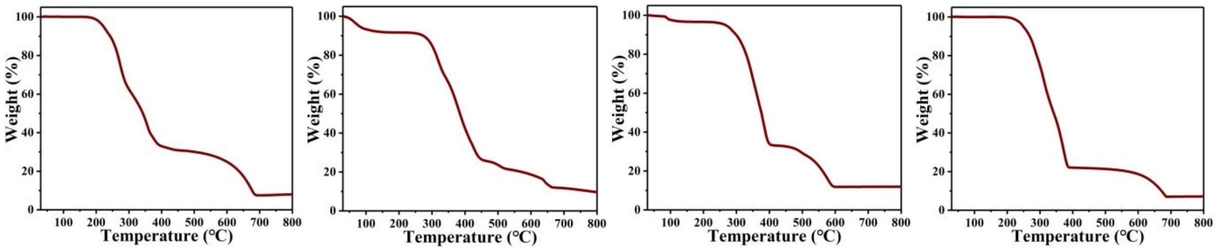

[BTEA]$_2$MnBr$_4$ (**9**) [TPA]$_2$MnCl$_4$ (**10**) [EPY]$_2$MnBr$_4$ (**11**) [CTMA]$_2$MnBr$_4$ (**12**)

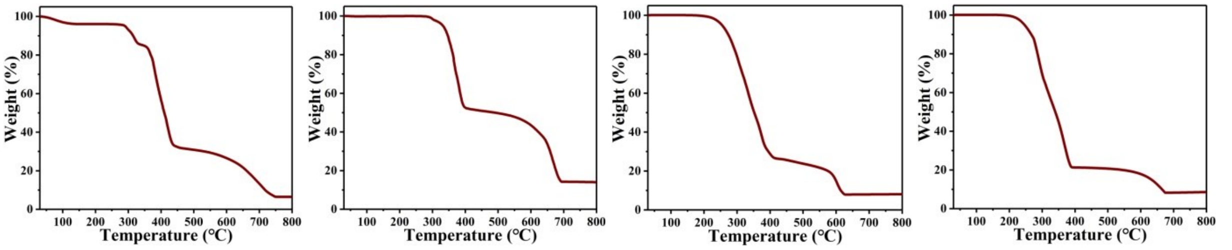

[EMPR]$_2$MnBr$_4$ (**13**) [DMPZ]MnBr$_4$ (**14**) [TTMA]$_2$MnBr$_4$ (**15**) [OTMA]$_2$MnBr$_4$ (**16**)

Fig. S9. The thermogravimetric analyses (TGA) curves for microscale hybrid manganese halides prepared from mechanical grinding solid-state reaction.

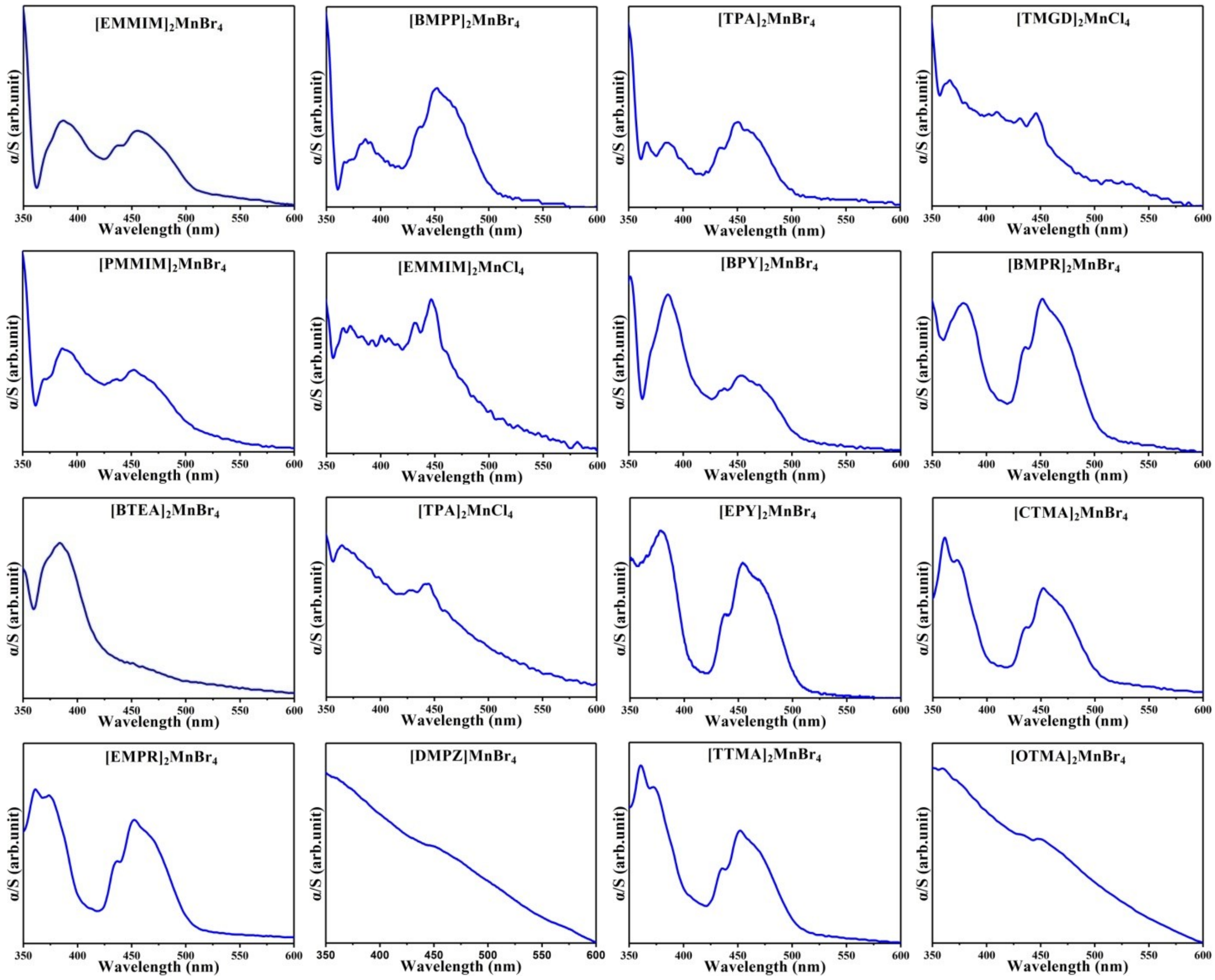

Fig. S10. The UV-Vis absorption spectra of microscale hybrid manganese halides prepared from mechanical grinding solid-state reaction.

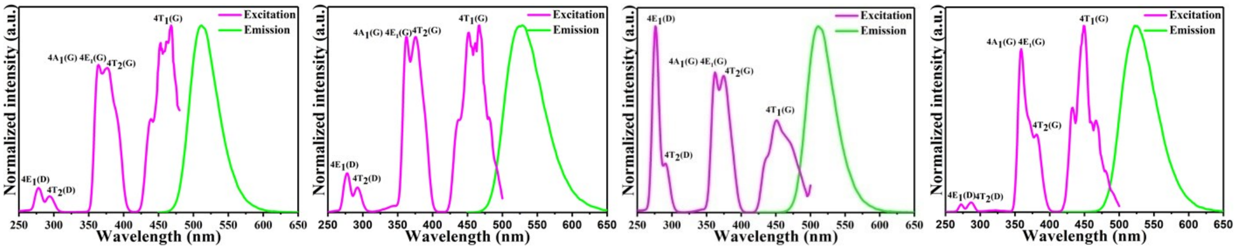

[EMMIM]$_2$MnBr$_4$ (**1**) [BMPP]$_2$MnBr$_4$ (**2**) [TPA]$_2$MnBr$_4$ (**3**) [TMGD]$_2$MnCl$_4$ (**4**)

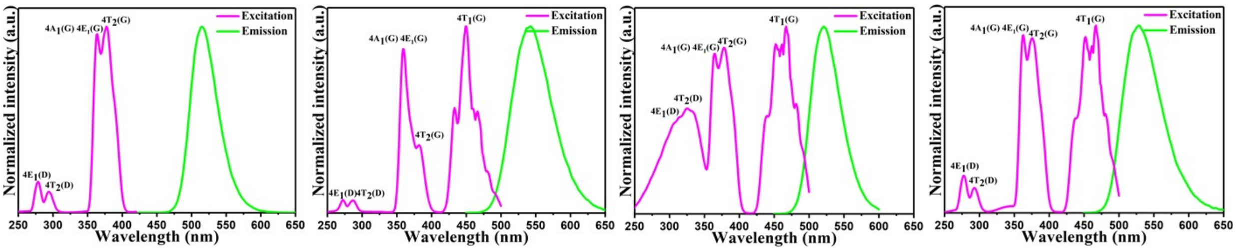

[PMMIM]$_2$MnBr$_4$ (**5**) [EMMIM]$_2$MnCl$_4$ (**6**) [BPY]$_2$MnBr$_4$ (**7**) [BMPR]$_2$MnBr$_4$ (**8**)

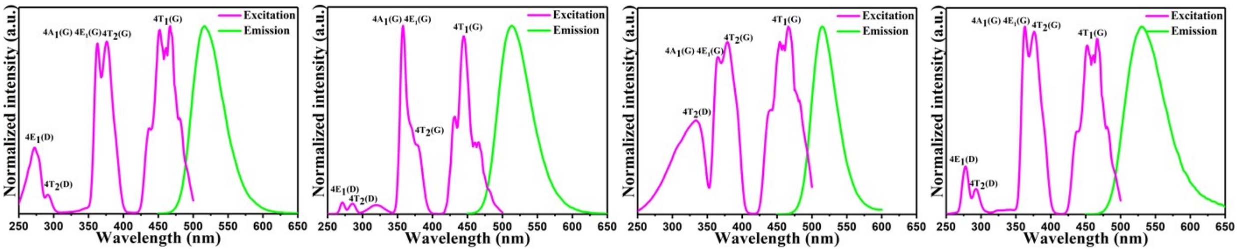

[BTEA]$_2$MnBr$_4$ (**9**) [TPA]$_2$MnCl$_4$ (**10**) [EPY]$_2$MnBr$_4$ (**11**) [CTMA]$_2$MnBr$_4$ (**12**)

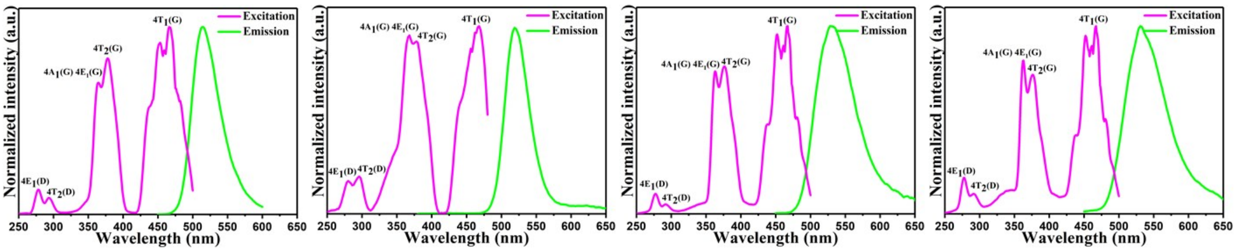

[EMPR]$_2$MnBr$_4$ (**13**) [DMPZ]MnBr$_4$ (**14**) [TTMA]$_2$MnBr$_4$ (**15**) [OTMA]$_2$MnBr$_4$ (**16**)

Fig. S11. The PL excitation and emission spectra of microscale 0D hybrid manganese halides prepared form mechanical grinding solid-state reaction.

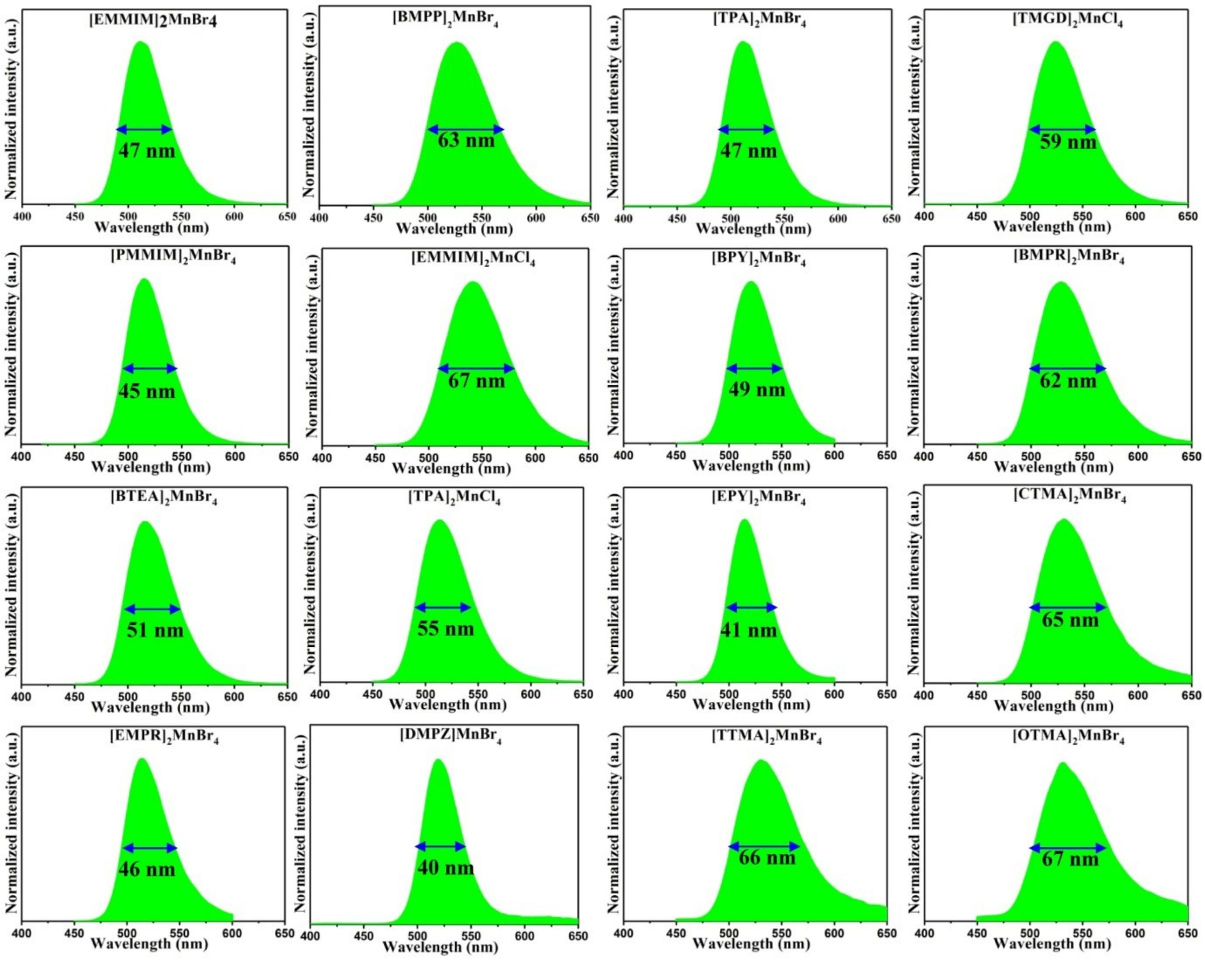

Fig. S12. The PL emission spectra and HWFM of microscale 0D hybrid manganese halides prepared form mechanical grinding solid-state reaction at 300 K.

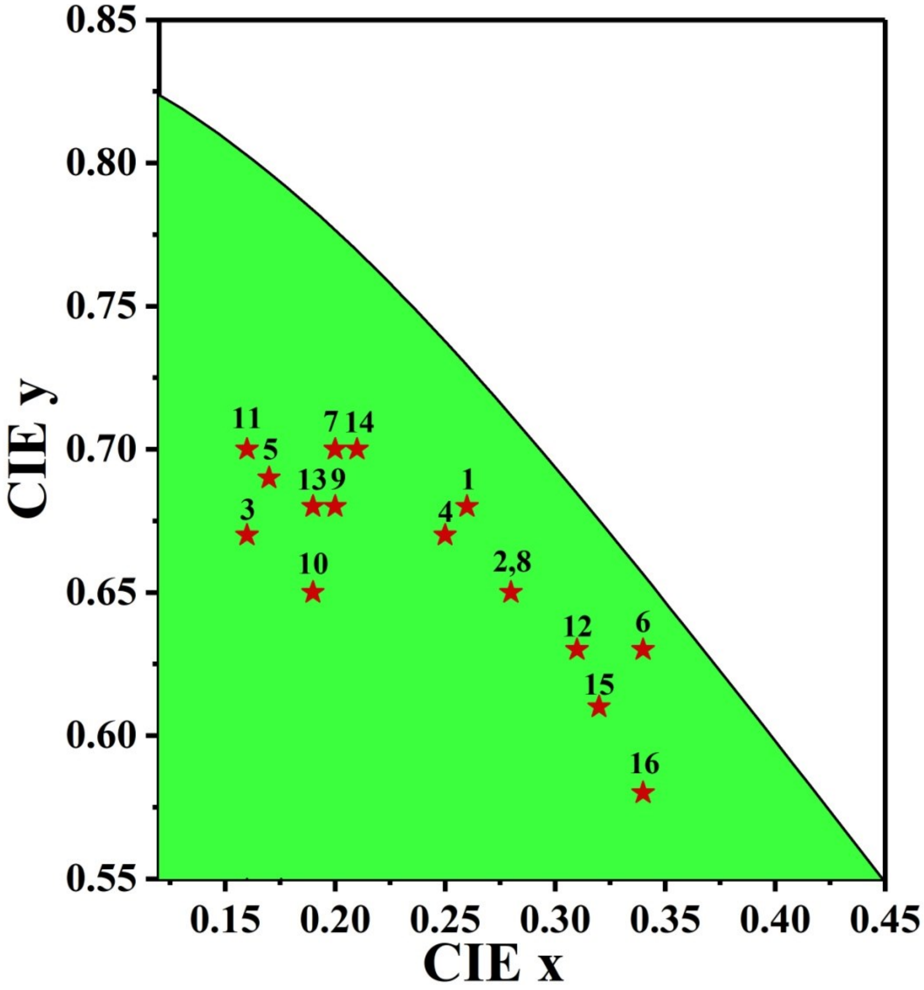

Fig. S13. The calculated Commission Internationale de l'Eclairage (CIE) chromaticity coordinates of microscale 0D hybrid manganese halides in this work: $[EMMIM]_2MnBr_4$ (**1**), $[BMPP]_2MnBr_4$ (**2**), $[TPA]_2MnBr_4$ (**3**), $[TMGD]_2MnCl_4$ (**4**), $[PMMIM]_2MnBr_4$ (**5**), $[EMMIM]_2MnCl_4$ (**6**), $[BPY]_2MnBr_4$ (**7**), $[BMPR]_2MnBr_4$ (**8**), $[BTEA]_2MnBr_4$ (**9**), $[TPA]_2MnCl_4$ (**10**), $[EPY]_2MnBr_4$ (**11**), $[CTMA]_2MnBr_4$ (**12**), $[EMPR]_2MnBr_4$ (**13**), $[DMPZ]MnBr_4$ (**14**), $[TTMA]_2MnBr_4$ (**15**) and $[OTMA]_2MnBr_4$ (**16**).

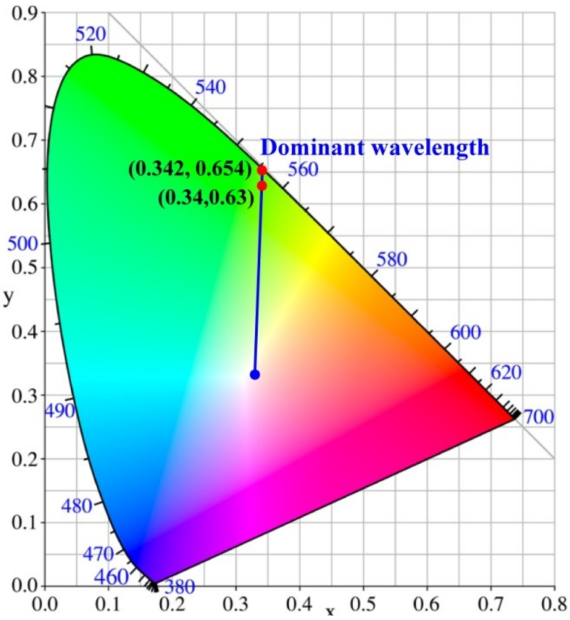

Fig. S14. The CIE chromaticity coordinates of $[EMMIM]_2MnCl_4$, corresponding dominant wavelength and equal-energy point in CIE-1931 color space.

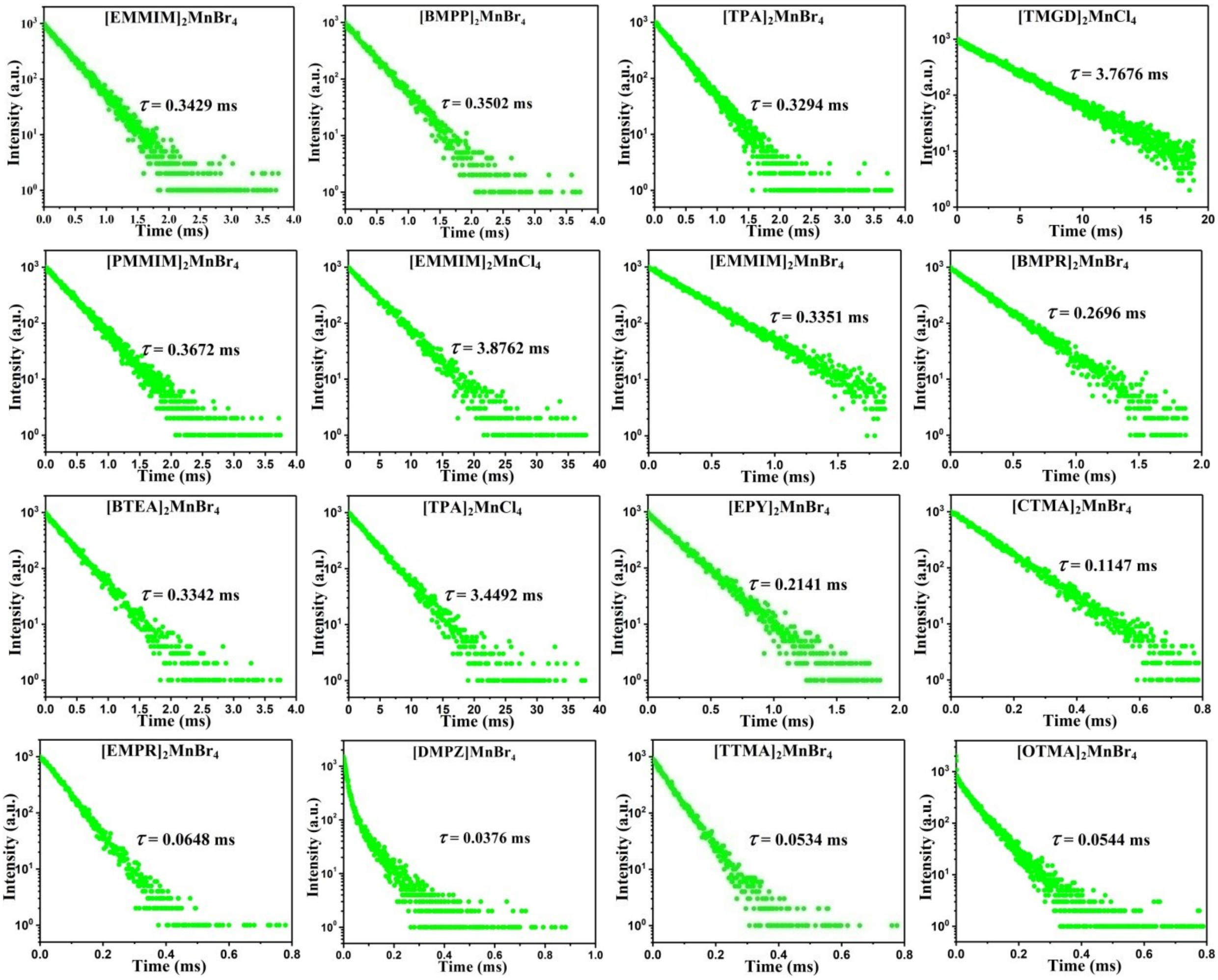

Fig. S15. The time-resolved PL decay curves of microscale hybrid manganese halides prepared form mechanical grinding solid-state reaction.

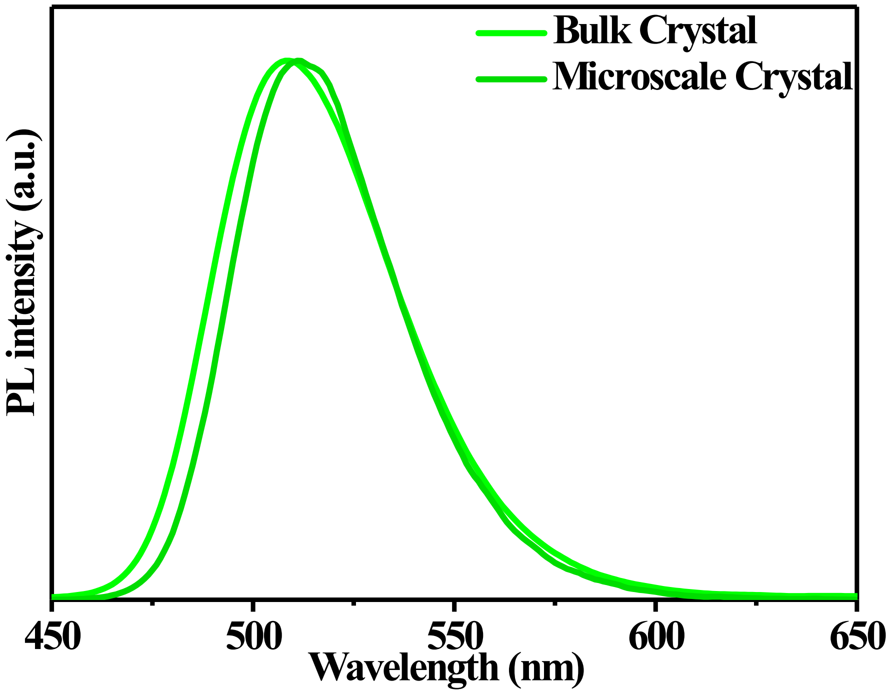

Fig. S16. Comparison of PL emission spectra of bulk and microscale $[EMMIM]_2MnBr_4$ crystals at 300 K.

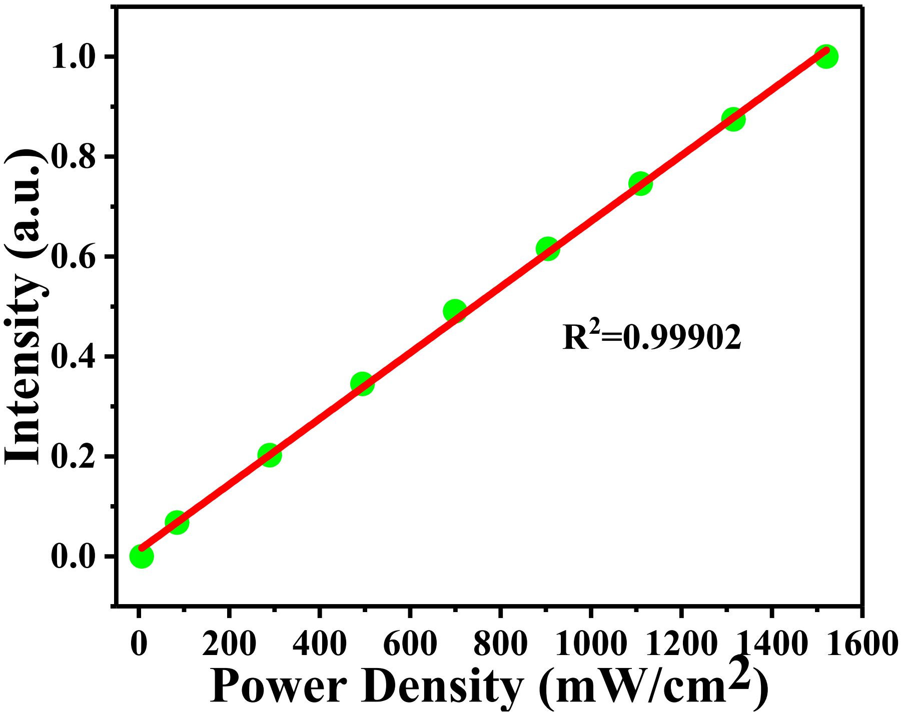

Fig. S17 Powder density dependent PL intensity of $[EMMIM]_2MnBr_4$ at 300K.

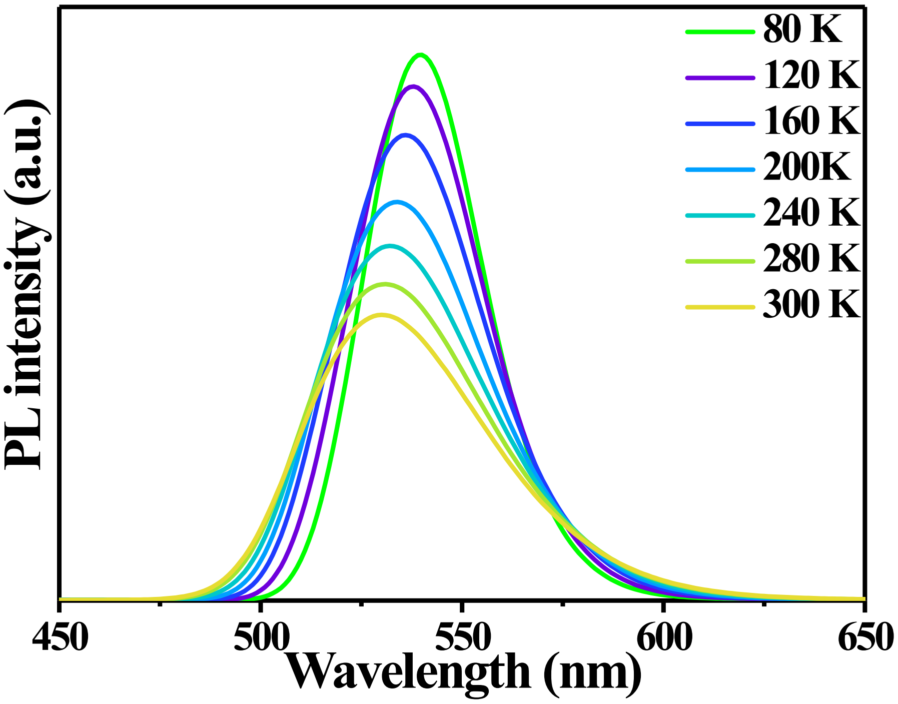

Fig. S18 Temperature-dependent emission spectra of $[EMMIM]_2MnBr_4$ from 80K to 300K.

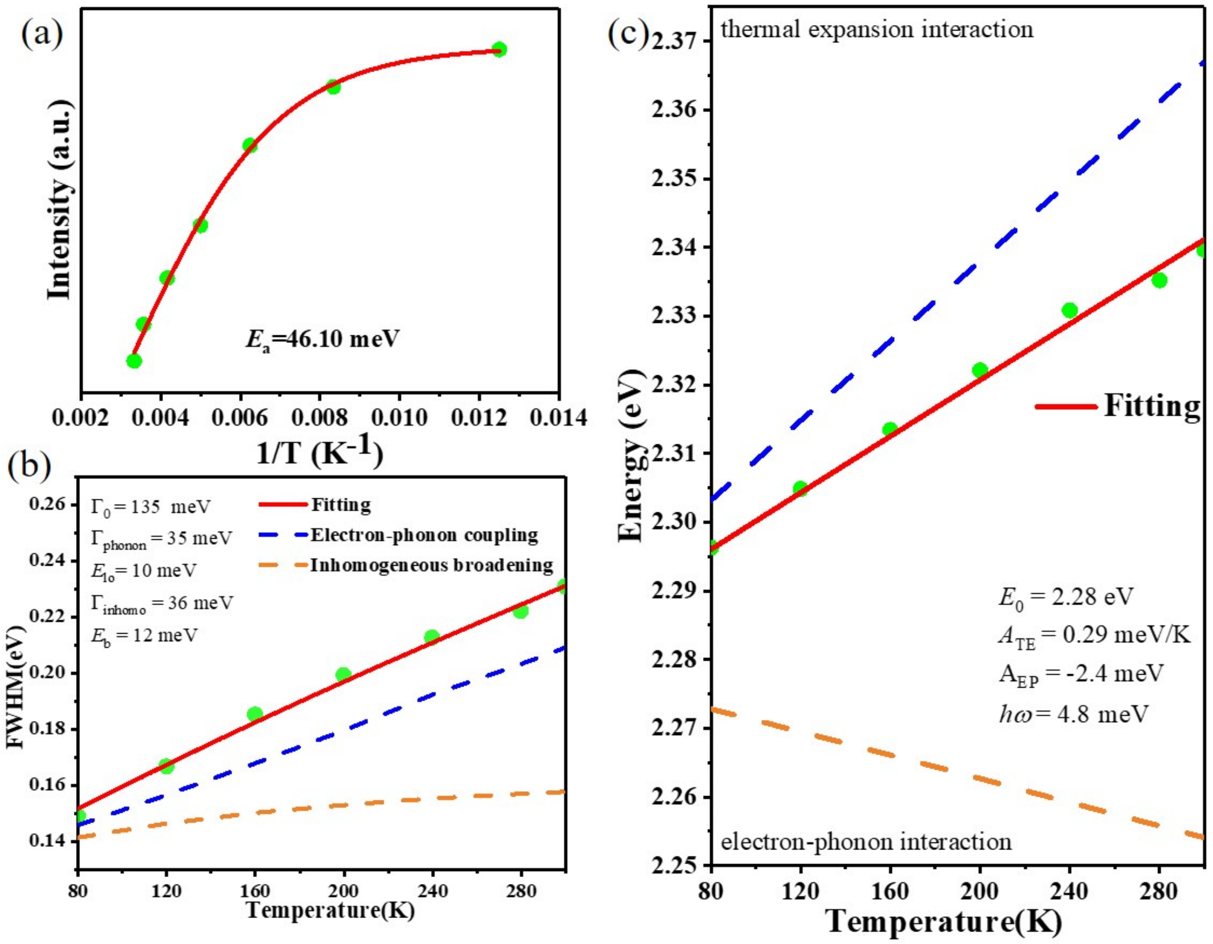

Fig. S19. Temperature dependence of (a) the PL intensity of $[EMMIM]_2MnBr_4$ and the theoretical fitting data from Arrhenius-type model, (b) the experimental and fitted FWHM of $[EMMIM]_2MnBr_4$ with the contribution of electron-phonon coupling and inhomogeneous broadening, (c) the PL energy evolution of $[EMMIM]_2MnBr_4$ with the contribution of thermal expansion and electronic-phonon interactions.

Note: The PL intensity of $[EMMIM]_2MnBr_4$ is fitted by using Arrhenius-type model:

$$I_{PL} = \frac{I_0}{1 + a\exp\left(\frac{-E_a}{k_B T}\right)}$$

where I_{PL} is the emission intensity at different temperature (T), I_0 is the integrated emission intensity at 0 K, E_a belongs to the activation energy related to the thermally activated non-radiation process, and k_B represents the Boltzmann constant.

The FWHM of $[EMMIM]_2MnBr_4$ with the contribution of electron-phonon coupling and inhomogeneous broadening according to the follow equation:

$$\Gamma(T) = \Gamma_0 + \Gamma_{\text{phonon}}(e^{E_{\text{LO}}/k_{\text{B}}T} - 1)^{-1} + \Gamma_{\text{inhomo}} e^{-E_{\text{b}}/k_{\text{B}}T}$$

where Γ_0 is the FWHM of 0 K, E_{LO} represents the energy of the longitudinal-optical phonon, E_{b} is the average binding energy of the trap states, Γ_{phonon} and Γ_{inhomo} represent the relative contribu-tions of electron-phonon coupling and trapped states induced inhomogeneous broadening, respectively.

The PL energy evolution is fitted according to the follow equation:

$$E_{\text{g}}(T) = E_0 + A_{\text{TE}}T + A_{\text{EP}}\left[\frac{2}{\exp\left(\frac{h\omega}{k_{\text{B}}}T\right) - 1} + 1\right]$$

where E_0 is the unrenormalized band gap, $E_{\text{g}}(T = 0) = E_0 + A_{\text{EP}}$; A_{TE} and A_{EP} are the weight of TE and EP interactions, respectively; $h\omega$ is the average optical phonon energy; and k_{B} is Boltzmann's constant.

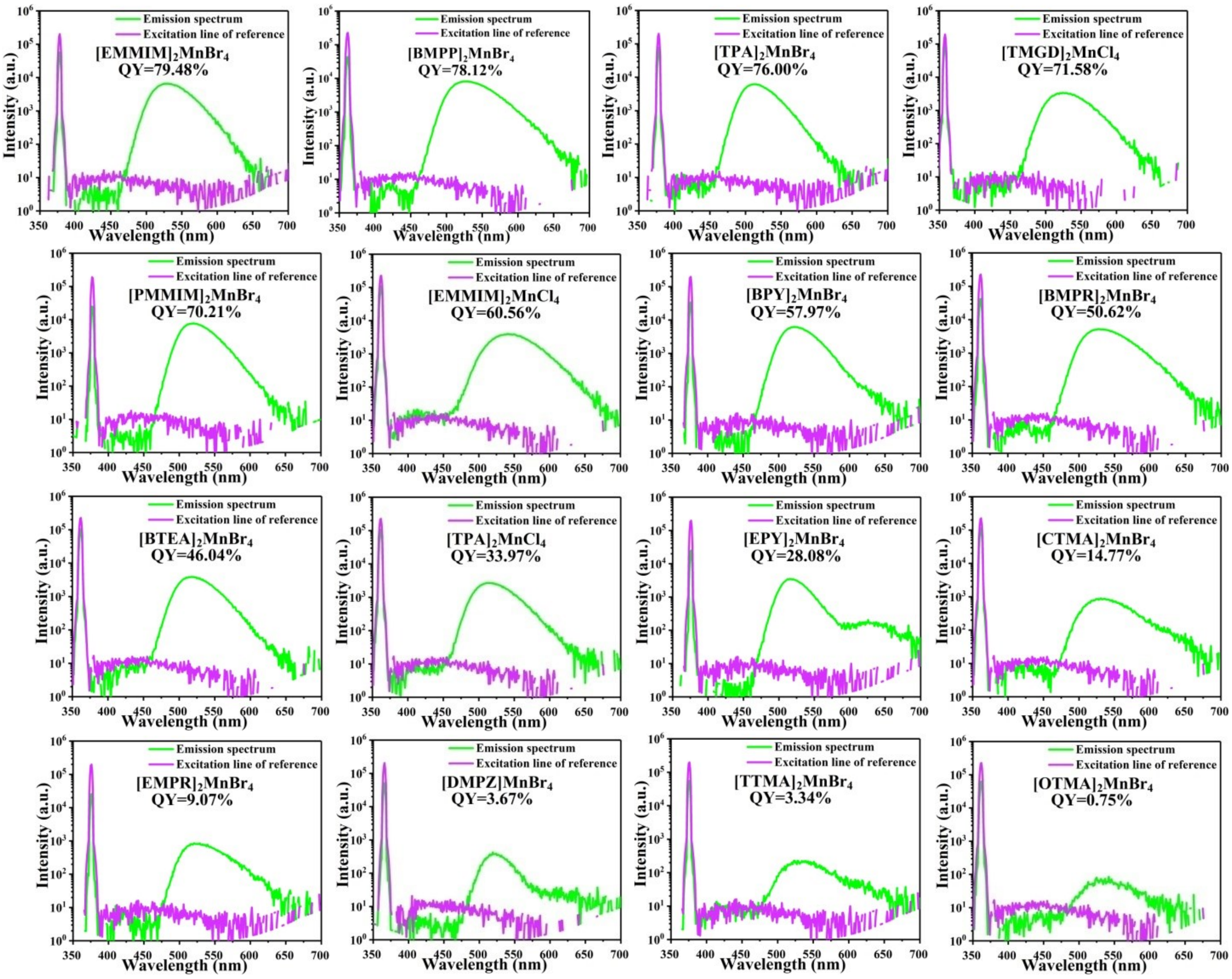

Fig. S20. The PLQYs of microscale 0D hybrid manganese halides prepared from mechanical grinding solid-state reaction.

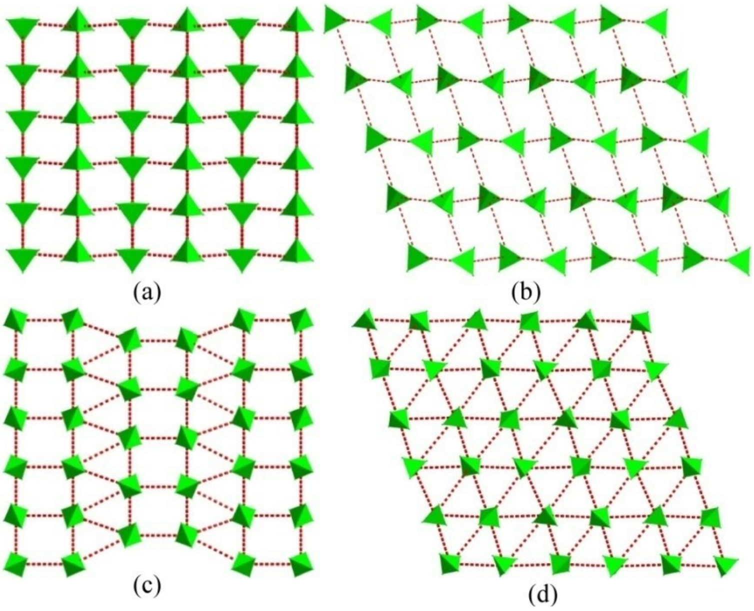

Fig. S21. Stacking patterns of tetrahedral $[MnX_4]^{2-}$ in hybrid manganese halides (the polyhedron represent $[MnX_4]^{2-}$ units).

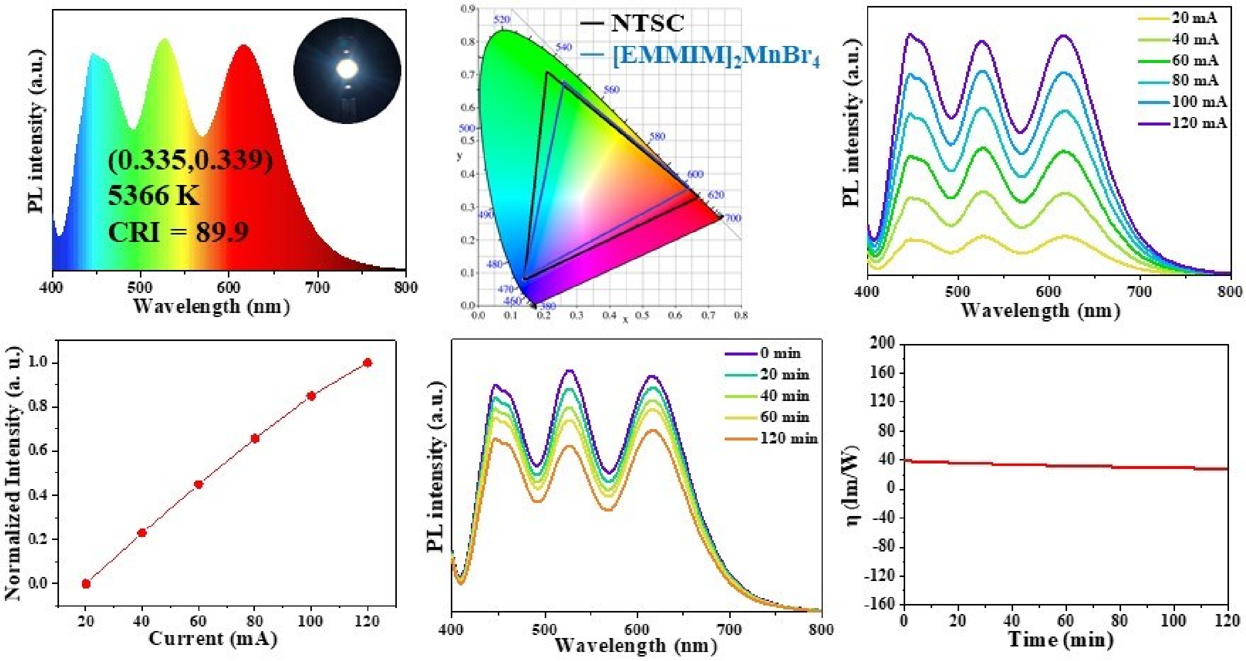

Fig. S22. (a) The PL spectra of white LED fabricated by microscale [EMMIM]$_2$MnBr$_4$ (1) green phosphor and commercial red phosphor $K_2SiF_6:Mn^{4+}$ and blue phosphor $BaMgAl_{10}O_{17}:Eu^{2+}$ on a UV LED chip at 20 mA drive current (inset: photograph of fabricated white LEDs), (b) color space of fabricated white LED LED (cyan) and color space of NTSC standard (black line) in CIE 1931 diagram; (c) Drive current dependent PL spectra of fabricated white LED device; (d) The normalized peak intensity variation of fabricated white LED under various operating currents; (e) The operating time-dependent PL spectra of fabricated white LED devices; (f) the operating time-dependent luminous efficiency of fabricated white LED devices.

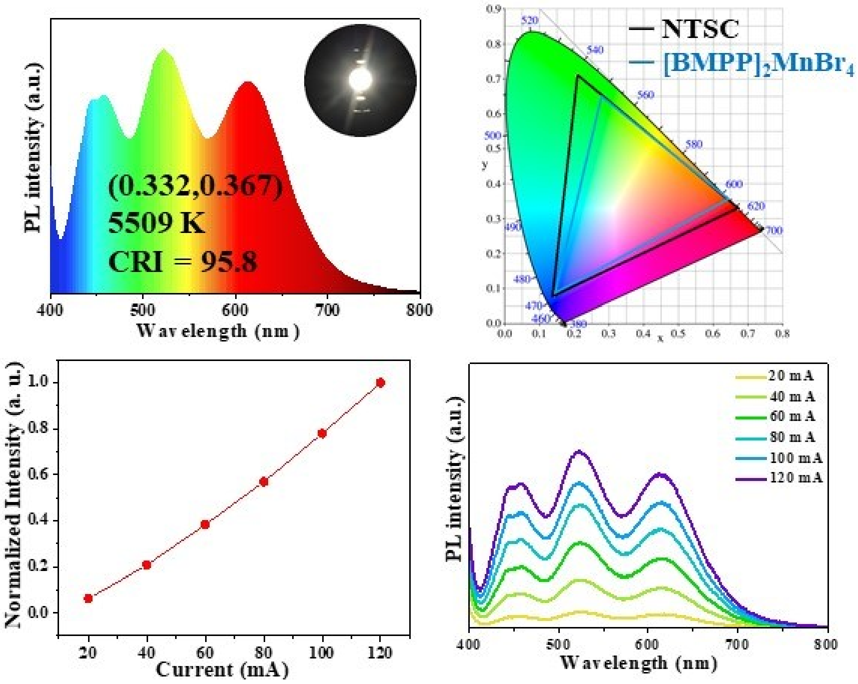

Fig. S23. (a) The PL spectra of white LED fabricated by microscale $[BMPP]_2MnBr_4$ (**2**) green phosphor and commercial red phosphor $K_2SiF_6:Mn^{4+}$ and blue phosphor $BaMgAl_{10}O_{17}:Eu^{2+}$ on a UV LED chip at 20 mA drive current (inset: photograph of fabricated white LEDs), (b) color space of fabricated white LED LED (cyan) and color space of NTSC standard (black line) in CIE 1931 diagram; (c) Drive current dependent PL spectra of fabricated white LED device; (d) The normalized peak intensity variation of fabricated white LED under various operating currents.

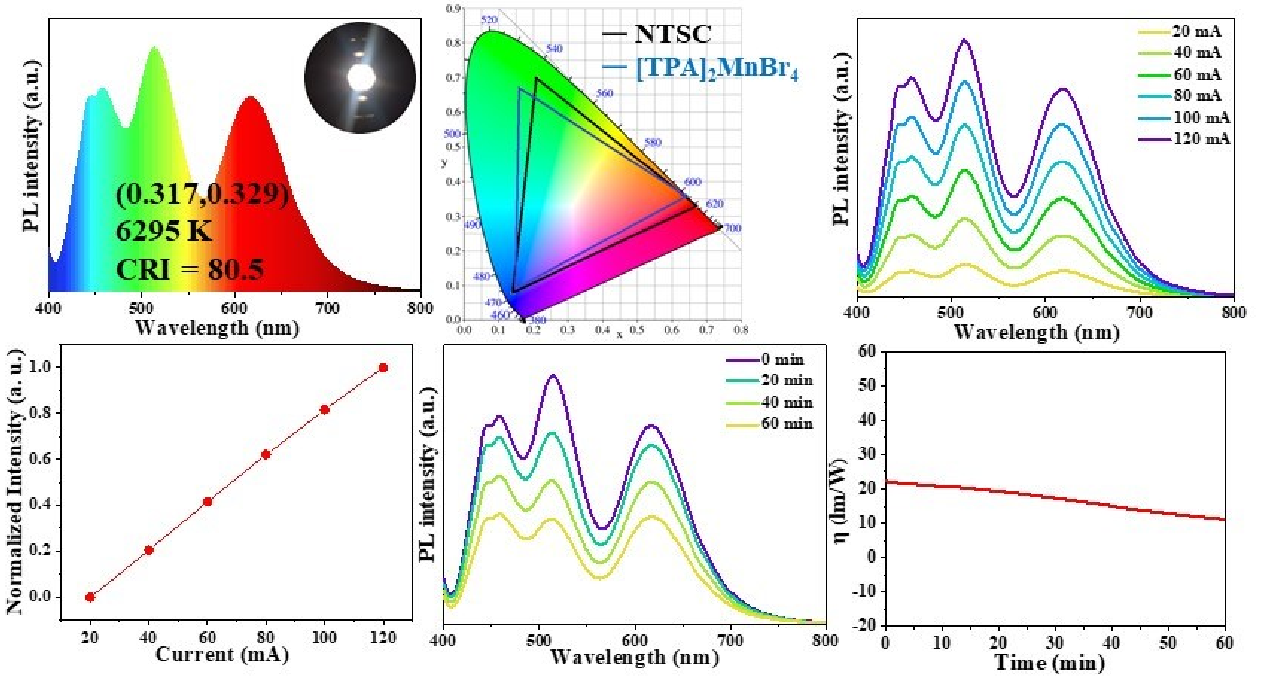

Fig. S24. (a) The PL spectra of white LED fabricated by microscale [TPA]$_2$MnBr$_4$ (**3**) green phosphor and commercial red phosphor $K_2SiF_6:Mn^{4+}$ and blue phosphor $BaMgAl_{10}O_{17}:Eu^{2+}$ on a UV LED chip at 20 mA drive current (inset: photograph of fabricated white LEDs), (b) color space of fabricated white LED LED (cyan) and color space of NTSC standard (black line) in CIE 1931 diagram; (c) Drive current dependent PL spectra of fabricated white LED device; (d) The normalized peak intensity variation of fabricated white LED under various operating currents; (e) The operating time-dependent PL spectra of fabricated white LED devices; (f) the operating time-dependent luminous efficiency of fabricated white LED devices.

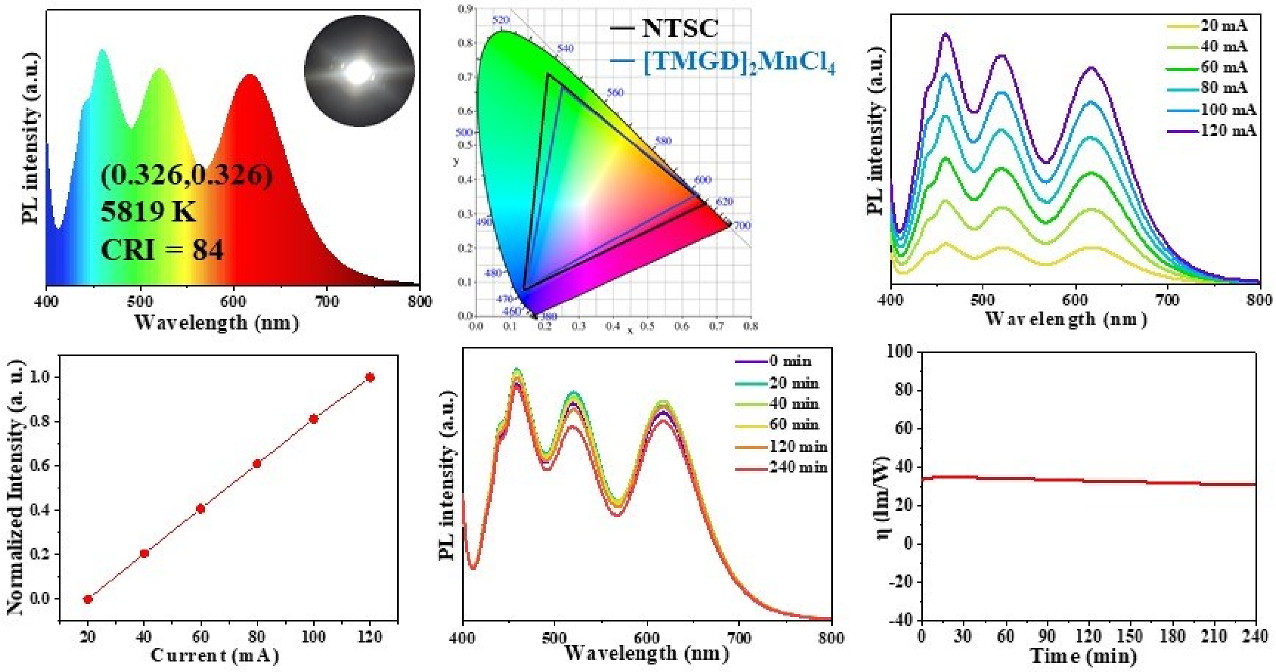

Fig. S25. (a) The PL spectra of white LED fabricated by microscale [TMGD]$_2$MnCl$_4$ (**4**) green phosphor and commercial red phosphor K_2SiF_6:Mn^{4+} and blue phosphor $BaMgAl_{10}O_{17}$:Eu^{2+} on a UV LED chip at 20 mA drive current (inset: photograph of fabricated white LEDs), (b) color space of fabricated white LED LED (cyan) and color space of NTSC standard (black line) in CIE 1931 diagram; (c) Drive current dependent PL spectra of fabricated white LED device; (d) The normalized peak intensity variation of fabricated white LED under various operating currents; (e) The operating time-dependent PL spectra of fabricated white LED devices; (f) the operating time-dependent luminous efficiency of fabricated white LED devices.

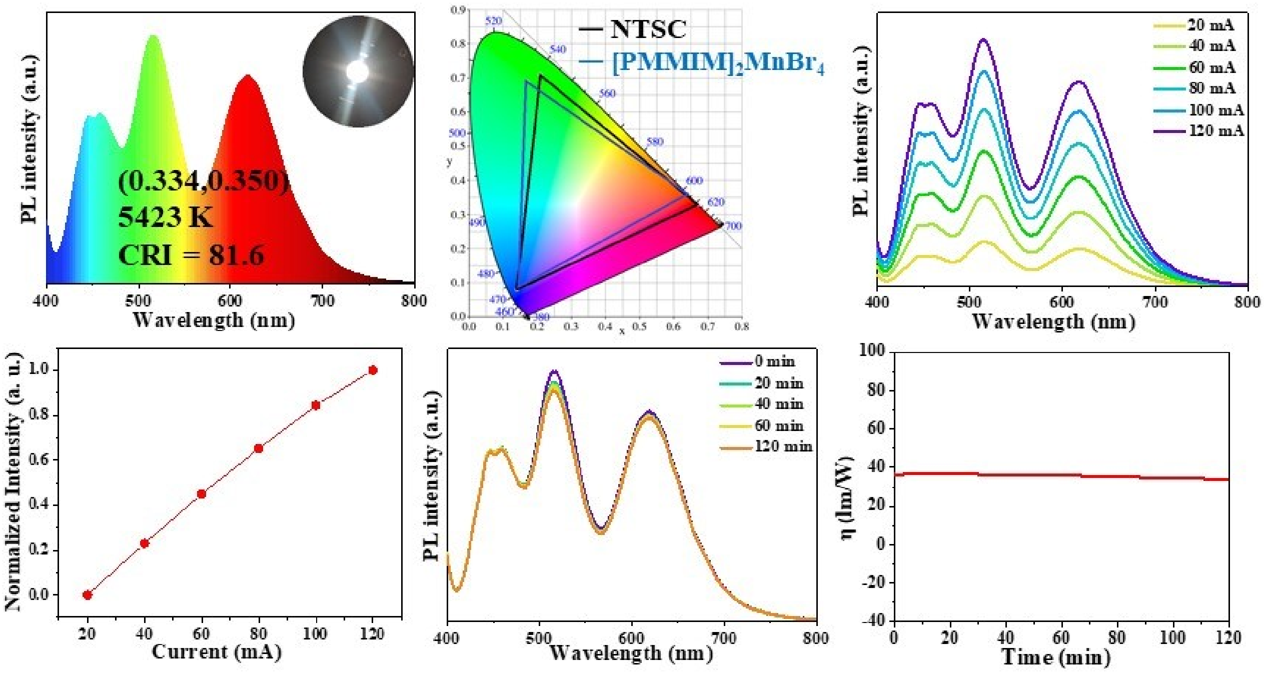

Fig. S26. (a) The PL spectra of white LED fabricated by microscale [PMMIM]$_2$MnBr$_4$ (**5**) green phosphor and commercial red phosphor $K_2SiF_6:Mn^{4+}$ and blue phosphor $BaMgAl_{10}O_{17}:Eu^{2+}$ on a UV LED chip at 20 mA drive current (inset: photograph of fabricated white LEDs), (b) color space of fabricated white LED LED (cyan) and color space of NTSC standard (black line) in CIE 1931 diagram; (c) Drive current dependent PL spectra of fabricated white LED device; (d) The normalized peak intensity variation of fabricated white LED under various operating currents; (e) The operating time-dependent PL spectra of fabricated white LED devices; (f) the operating time-dependent luminous efficiency of fabricated white LED devices.

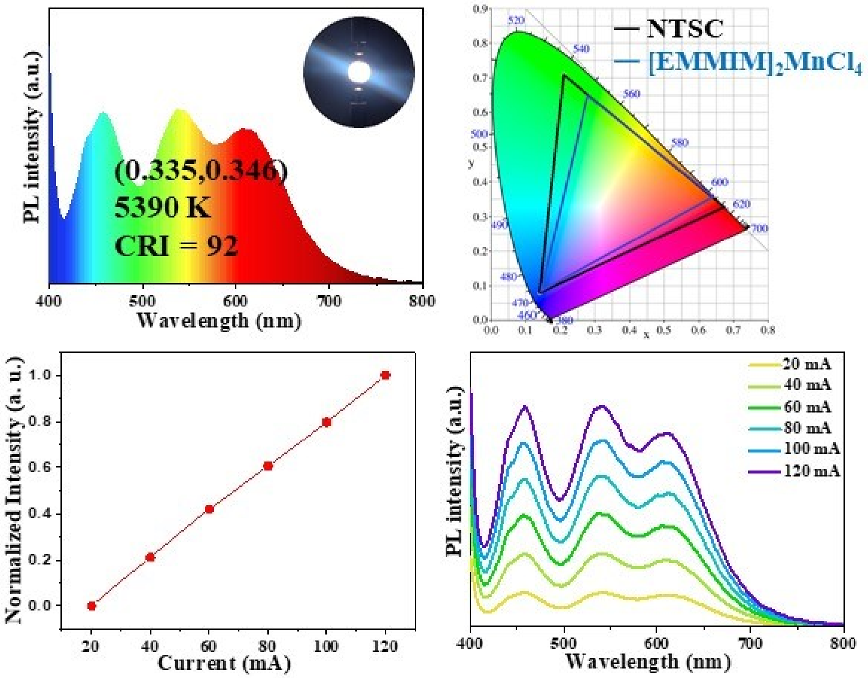

Fig. S27. (a) The PL spectra of white LED fabricated by microscale [EMMIM]$_2$MnCl$_4$ (**6**) green phosphor and commercial red phosphor K_2SiF_6:Mn^{4+} and blue phosphor $BaMgAl_{10}O_{17}$:Eu^{2+} on a UV LED chip at 20 mA drive current (inset: photograph of fabricated white LEDs), (b) color space of fabricated white LED LED (cyan) and color space of NTSC standard (black line) in CIE 1931 diagram; (c) Drive current dependent PL spectra of fabricated white LED device; (d) The normalized peak intensity variation of fabricated white LED under various operating currents.

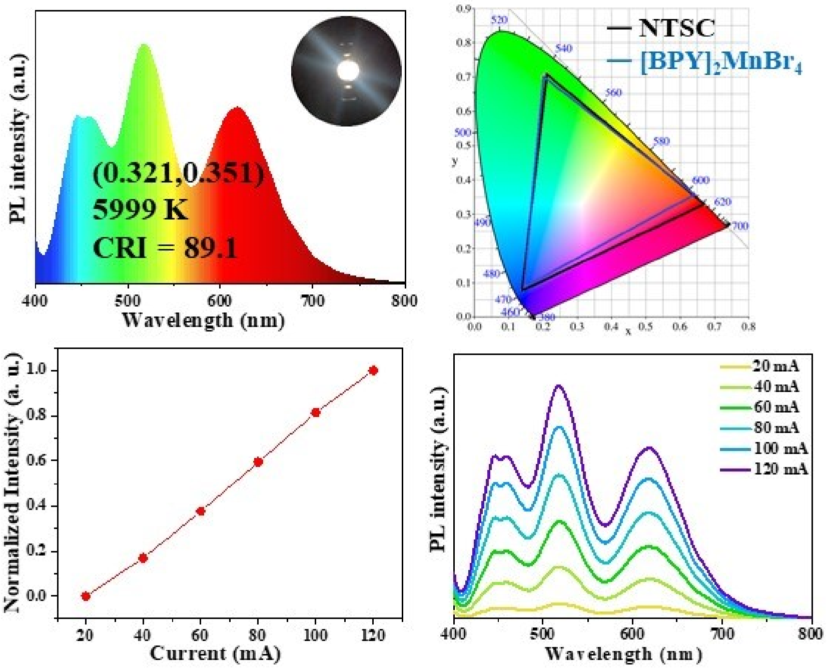

Fig. S28. (a) The PL spectra of white LED fabricated by microscale $[BPY]_2MnBr_4$ (**7**) green phosphor and commercial red phosphor $K_2SiF_6:Mn^{4+}$ and blue phosphor $BaMgAl_{10}O_{17}:Eu^{2+}$ on a UV LED chip at 20 mA drive current (inset: photograph of fabricated white LEDs), (b) color space of fabricated white LED LED (cyan) and color space of NTSC standard (black line) in CIE 1931 diagram; (c) Drive current dependent PL spectra of fabricated white LED device; (d) The normalized peak intensity variation of fabricated white LED under various operating currents.

Table S2. The full and abbreviated name of organic salt used in this work.

Abbreviation	**Full name**
[EMMIM] Br	1-ethyl-2,3-dimethylimidazolium bromide
[BMPP]Br	1-butyl-1-methylpiperidinium bromide
[TPA]Br	tetrapropylammonium bromide
[TMGD]Cl	tetraMethylguanidine chloride
[PMMIM]Br	1-propyl-2,3-dimethylimidazolium bromide
[EMMIM]Cl	1-ethyl-2,3-dimethylimidazolium chloride
[BPY]Br	1-butylpyridinium bromide
[BMPR]Br	1-butyl-1-methylpyrrolidinium bromide
[BTEA]Br	benzyltriethylammonium bromide
[TPA]Cl	tetrapropyl ammonium chloride
[EPY]Br	1-ethylpyridinium bromide
[CTMA]Br	cetyltrimethylammonium bromide
[EMPR]Br	1-ethyl-1-methylpyrrolidinium bromide
[DMPZ]Br_2	N,N'-dimethylpiperazine bromide
[TTMA]Br	tetradecyltrimethylammonium bromide
[OTMA]Br	octadecyltrimethylammonium bromide

Table S3. The ICP-OES results for all microscale hybrid manganese halides.

Compounds	molecular formula	Mn	
		Calcd.	Found
$[EMMIM]_2MnBr_4$	$C_{14}N_4H_{26}MnBr_4$	8.79%	8.89%
$[BMPP]_2MnBr_4$	$C_{20}N_2H_{44}MnBr_4$	8.00%	7.95%
$[TPA]_2MnBr_4$	$C_{24}N_2H_{56}MnBr_4$	7.35%	7.42%
$[TMGD]_2MnCl_4$	$C_{10}N_6H_{28}MnCl_4$	12.80%	12.89%
$[PMMIM]_2MnBr_4$	$C_{16}N_4H_{30}MnBr_4$	8.41%	8.32%
$[EMMIM]_2MnCl_4$	$C_{14}N_4H_{26}MnCl_4$	12.29%	12.20%
$[BPY]_2MnBr_4$	$C_{18}N_2H_{28}MnBr_4$	8.49%	8.53%
$[BMPR]_2MnBr_4$	$C_{18}N_2H_{40}MnBr_4$	8.34%	8.21%
$[BTEA]_2MnBr_4$	$C_{26}N_2H_{44}MnBr_4$	7.24%	7.36%
$[TPA]_2MnCl_4$	$C_{24}N_2H_{56}MnCl_4$	9.65%	9.52%
$[EPY]_2MnBr_4$	$C_{14}N_2H_{20}MnBr_4$	9.30%	9.41%
$[CTMA]_2MnBr_4$	$C_{38}N_2H_{84}MnBr_4$	5.82%	5.98%
$[EMPR]_2MnBr_4$	$C_{14}N_2H_{32}MnBr_4$	9.11%	9.23%
$[DMPZ]MnBr_4$	$C_6N_2H_{16}MnBr_4$	11.19%	11.06%
$[TTMA]_2MnBr_4$	$C_{34}N_2H_{76}MnBr_4$	6.19%	6.25%
$[OTMA]_2MnBr_4$	$C_{42}N_2H_{92}MnBr_4$	5.50%	5.62%

Table S4. The elemental analysis results for all the microscale hybrid manganese halides.

Compounds	molecular formula	C		N		H	
		Calcd.	Found	Calcd.	Found	Calcd.	Found
$[EMMIM]_2MnBr_4$	$C_{14}N_4H_{26}MnBr_4$	26.9%	27.3%	8.96%	9.32%	4.19%	4.40%
$[BMPP]_2MnBr_4$	$C_{20}N_2H_{44}MnBr_4$	35.0%	35.3%	4.08%	4.39%	6.45%	6.61%
$[TPA]_2MnBr_4$	$C_{24}N_2H_{56}MnBr_4$	38.6%	38.4%	3.74%	3.46%	7.55%	7.27%
$[TMGD]_2MnCl_4$	$C_{10}N_6H_{28}MnCl_4$	28.0%	28.2%	19.6%	19.9%	6.58%	6.81%
$[PMMIM]_2MnBr_4$	$C_{16}N_4H_{30}MnBr_4$	29.4%	29.3%	8.58%	8.64%	4.63%	4.69%
$[EMMIM]_2MnCl_4$	$C_{14}N_4H_{26}MnCl_4$	37.6%	37.4%	12.5%	12.4%	5.86%	5.80%
$[BPY]_2MnBr_4$	$C_{18}N_2H_{28}MnBr_4$	33.4%	33.9%	4.33%	4.67%	4.36%	4.59%
$[BMPR]_2MnBr_4$	$C_{18}N_2H_{40}MnBr_4$	32.8%	33.0%	4.25%	4.39%	6.12%	6.43%
$[BTEA]_2MnBr_4$	$C_{26}N_2H_{44}MnBr_4$	41.1%	40.8%	3.69%	3.51%	5.84%	5.63%
$[TPA]_2MnCl_4$	$C_{24}N_2H_{56}MnCl_4$	50.6%	50.9%	4.92%	5.01%	9.91%	10.2%
$[EPY]_2MnBr_4$	$C_{14}N_2H_{20}MnBr_4$	28.5%	28.4%	4.74%	4.65%	3.41%	3.29%
$[CTMA]_2MnBr_4$	$C_{38}N_2H_{84}MnBr_4$	48.4%	48.6%	2.97%	3.01%	8.97%	9.13%
$[EMPR]_2MnBr_4$	$C_{14}N_2H_{32}MnBr_4$	27.9%	28.3%	4.65%	4.93%	5.35%	5.68%
$[DMPZ]MnBr_4$	$C_6N_2H_{16}MnBr_4$	14.7%	14.8%	5.71%	5.79%	3.29%	3.33%
$[TTMA]_2MnBr_4$	$C_{34}N_2H_{76}MnBr_4$	46.0%	45.9%	3.16%	3.02%	8.63%	8.50%
$[OTMA]_2MnBr_4$	$C_{42}N_2H_{92}MnBr_4$	50.5%	50.8%	2.80%	2.96%	9.28%	9.45%

Table S5. The emission CIE of microscale hybrid manganese halides and corresponding dominant wavelength as well as the color purity.

	Compound	CIE	Dominant CIE	CP
1	$[EMMIM]_2MnBr_4$	(0.26,0.68)	(0.25, 0.74)	86%
2	$[BMPP]_2MnBr_4$	(0.28,0.65)	(0.27, 0.72)	82%
3	$[TPA]_2MnBr_4$	(0.16,0.67)	(0.08, 0.83)	67%
4	$[TMGD]_2MnCl_4$	(0.25,0.67)	(0.23, 0.75)	80%
5	$[PMMIM]_2MnBr_4$	(0.17,0.69)	(0.11, 0.83)	72%
6	$[EMMIM]_2MnCl_4$	(0.34,0.63)	(0.34, 0.65)	93%
7	$[BPY]_2MnBr_4$	(0.20,0.70)	(0.17, 0.80)	79%
8	$[BMPR]_2MnBr_4$	(0.28,0.65)	(0.27, 0.72)	82%
9	$[BTEA]_2MnBr_4$	(0.20,0.68)	(0.15, 0.81)	74%
10	$[TPA]_2MnCl_4$	(0.19,0.65)	(0.11, 0.83)	64%
11	$[EPY]_2MnBr_4$	(0.16,0.70)	(0.10, 0.83)	74%
12	$[CTMA]_2MnBr_4$	(0.31,0.63)	(0.31, 0.69)	84%
13	$[EMPR]_2MnBr_4$	(0.19,0.68)	(0.14, 0.82)	72%
14	$[DMPZ]MnBr_4$	(0.21,0.70)	(0.18, 0.79)	80%
15	$[TTMA]_2MnBr_4$	(0.32,0.61)	(0.32, 0.68)	80%
16	$[OTMA]_2MnBr_4$	(0.34,0.58)	(0.34, 0.65)	78%

Table S6. Summary of the photophysical parameters of previously reported green-light emitting 0D manganese halides.

Material	Emission	PLQY	FWHM	Lifetime	Ref.
$[Ph_4P]_2MnBr_4$	516 nm	98 %	……	0.355 ms	1
$(TMPEA)_2MnBr_4$	520 nm	98 %	……	0.096 ms	2
$(ETPP)MnBr_4$	517 nm	95 %	51 nm	0.318 ms	3
$LMnCl_4$	530 nm	92.3%	……	1.54 ms	4
$(TPA)_2MnBr_4$	512 nm	89.2 %	……	……	5
$(BTMA)_2MnBr_4$	518 nm	88.8 %	46 nm	0.33 ms	6
$(BTMA)_2MnBr_4$,	516 nm	88.5 %	48 nm	……	7
$[P14]MnBr_4$	520 nm	81 %	55 nm	0.358 ms	8
$(Bmpy)_2MnBr_4$	528 nm	80.1 %	64 nm	0.326 ms	9
$[EMMIM]_2MnBr_4$	511nm	79.5%	47 nm	0.3429 ms	This work
$(MPip)MnCl_4$	530 nm	79.4 %	60 nm	0.715 ms	10
$(TEA)_2MnBr_4$	516 nm	78.9 %	……	……	5
$[BMPP]_2MnBr_4$	530 nm	78.1%	63 nm	0.3502 ms	This work
$(Bz(Me)_3N)_2MnCl_4$	547 nm	78 %	71.8nm	3.79 ms	11
$[TPA]_2MnBr_4$	511 nm	76.0%	47 nm	0.3294 ms	This work
$(BTMA)_2MnBr_4$	514 nm	72.3 %	……	0.236 ms	12
$[TMGD]_2MnBcCl_4$	525nm	71.6%	59 nm	3.7676 ms	This work
$(btmdme)_2MnCl_4$	516 nm	71.3 %	……	……	5
$(EMMIm)_2MnCl_4$	536 nm	70.8	……	3.90 ms	13
$[PMMIM]_2MnBr_4$	515 nm	70.2%	45 nm	0.3672 ms	This work
$(Bz(Me)_3N)_2MnBr_4$	516 nm	63 %	48.7nm	0.34 ms	11
$DIPA_2MnBr_4$	525 nm	62 %	62.9 nm	1.44 ns	14
$[EMMIM]_2MnCl_4$	539 nm	60.6%	67 nm	3.880 ms	This work
$[BPY]_2MnBr_4$	521 nm	58.0%	49 nm	0.3351 ms	This work
$[PP14]MnBr_4$	527 nm	55 %	64 nm	0.361 ms	8
$(IPTMA)_2MnBr_4$	497 nm	52.6 %	……	……	15

$[Py]_2MnBr_4$	525 nm	51.4 %	……	……	16
$[BMPR]_2MnBr_4$	527 nm	50.6%	62 nm	0.2629 ms	This work
Cs_3MnBr_5	520 nm	49 %	42 nm	0.29 ms	17

Table S7. Summary of the photophysical parameters of single crystalline lead halides and perovskite quantum dots or nanomaterials.

Material	Emission	PLQY	FWHM	Lifetime	Ref.
$[bmpy]_9[ZnCl_4]_2[Pb_3Cl_{11}]$	512 nm	~ 100%	61.3 nm	0.54 μs	18
$FAPbBr_3$ film	530 nm	92%	22 nm	24.2 ns	26
$Cs_3Cu_2Cl_5$	515 nm	91.30%	91 nm	112.4 μs	27
$[bmpy]_9Pb_3Zn_2Cl_{19}$	516 nm	91%	61 nm	569 ns	19
$FAPbBr_3$ nanoplate	530 nm	85%	25.3nm	12 ns	25
$CsPbBr_3$	507 nm	80%	23 nm	6.6ns	23
$[EMMIM]_2MnBr_4$	511nm	79.50%	47 nm	0.3429 ms	This work
$[BMPP]_2MnBr_4$	530 nm	78.10%	63 nm	0.3502 ms	This work
$[TPA]_2MnBr_4$	511 nm	76.00%	47 nm	0.3294 ms	This work
$[TMGD]_2MnBcCl_4$	525nm	71.60%	59 nm	3.7676 ms	This work
$[PMMIM]_2MnBr_4$	515 nm	70.20%	45 nm	0.3672 ms	This work
$[EMMIM]_2MnCl_4$	539 nm	60.60%	67 nm	3.880 ms	This work
$[BPY]_2MnBr_4$	521 nm	58.00%	49 nm	0.3351 ms	This work
$[BMPR]_2MnBr_4$	527 nm	50.60%	62 nm	0.2629 ms	This work
$[bmpy]_9[MnBr_4]_2[Pb_3Br_{11}]$	528 nm	49.80%	67 nm	114.3μs	20
$[bmpy]_6Pb_3Br_{12}$	522 nm	12%	134 nm	36.78ns	21
$[bmpy]_9[ZnBr_4]_2[Pb_3Br_{11}]$	564 nm	7%	68 nm	36 ns	22
$MAPbBr_3$ film	532 nm	-	15.3nm	15.28ns	24

Table S8. Summary of the photophysical parameters of representative commercial inorganic green phosphors.

Material	Emission	PLQY	FWHM	Lifetime	Ref.
β-SiAlON:Eu^{2+}	538 nm	96.50%	53 nm	1 μs	28
$SrGa_2S_4$:Eu^{2+}	540 nm	95%	47 nm	-	34
$Ba[Li_2(Al_2Si_2)N_6]$:Eu^{2+}	532 nm	80%	57 nm	-	31
$RbLi(Li_3SiO_4)_2$:Eu^{2+}	530 nm	80%	42 nm	-	33
$[EMMIM]_2MnBr_4$	511nm	79.50%	47 nm	0.3429 ms	This work
$Ba_2LiSi_7AlN_{12}$:Eu^{2+}	515nm	79%	61 nm	0.6 μs	32
$[BMPP]_2MnBr_4$	530 nm	78.10%	63 nm	0.3502 ms	This work
$[TPA]_2MnBr_4$	511 nm	76.00%	47 nm	0.3294 ms	This work
$Sr_2MgAl_{22}O_{36}$:Mn^{2+}	518 nm	75%	26 nm	4.71 ms	30
$[TMGD]_2MnBcCl_4$	525nm	71.60%	59 nm	3.7676 ms	This work
$[PMMIM]_2MnBr_4$	515 nm	70.20%	45 nm	0.3672 ms	This work
$[EMMIM]_2MnCl_4$	539 nm	60.60%	67 nm	3.880 ms	This work
$[BPY]_2MnBr_4$	521 nm	58.00%	49 nm	0.3351 ms	This work
$[BMPR]_2MnBr_4$	527 nm	50.60%	62 nm	0.2629 ms	This work
$MgAl_2O_4$:Mn^{2+}	525 nm	45%	35 nm	6.51 ms	29

Table S9. Summary of photoluminescence parameters of bulk 0D hybrid manganese halides prepared from wet-chemistry solution crystallization method.

	Compound	λ_{em} (nm)	CIE	FWHM (nm)	CP	PLQY
1	$[EMMIM]_2MnBr_4$	528	(0.26,0.68)	51	86%	68.49%
2	$[BMPP]_2MnBr_4$	522	(0.25,0.67)	58	80%	73.63%
3	$[TPA]_2MnBr_4$	511	(0.15,0.66)	45	66%	51.16%
4	$[TMGD]_2MnCl_4$	520	(0.22,0.68)	45	77%	79.43%
5	$[PMMIM]_2MnBr_4$	516	(0.18,0.69)	46	73%	63.92%
6	$[EMMIM]_2MnCl_4$	536	(0.31,0.65)	63	90%	71.99%
7	$[BPY]_2MnBr_4$	517	(0.18,0.69)	48	73%	64.18%
8	$[BMPR]_2MnBr_4$	525	(0.26,0.67)	59	83%	75.50%
9	$[BTEA]_2MnBr_4$	514	(0.17,0.69)	47	72%	64.89%
10	$[TPA]_2MnCl_4$	510	(0.14,0.03)	50	64%	64.17%
11	$[EPY]_2MnBr_4$	513	(0.17,0.68)	40	70%	44.15%
12	$[CTMA]_2MnBr_4$	......	......	......	......	......
13	$[EMPR]_2MnBr_4$	525	(0.27,0.65)	59	79%	8.16%
14	$[DMPZ]MnBr_4$	518	(0.17,0.57)	45	53%	13.96%
15	$[TTMA]_2MnBr_4$	......	......	......	......	......
16	$[OTMA]_2MnBr_4$	......	......	......	......	......

Table S10. Summaries of the Mn···Mn distances and PLQYs of bulk 0D hybrid manganese bromides obtained from wet-chemistry solution crystallization method.

Compound	**Mn···Mn distances (Å)**						**PLQY**
[DMPZ]$_2$MnBr$_4$	**6.354**	6.945	8.019	8.097	······	······	**13.96%**
[EPY]$_2$MnBr$_4$	**6.871**	8.186	8.341	9.422	9.852	9.761	**44.15%**
[PMMIM]$_2$MnBr$_4$	**8.186**	9.447	9.645	9.942	10.385	······	**63.92%**
[BPY]$_2$MnBr$_4$	**8.459**	9.027	9.327	9.365	9.477	9.678	**64.18%**
[EMMIM]$_2$MnBr	**8.588**	8.921	9.088	9.435	9.649	9.806	**68.49%**
[BMPR]$_2$MnBr$_4$	**9.254**	9.584	9.650	9.868	10.003	10.243	**75.50%**
[BMPP]$_2$MnBr	**9.528**	9.821	9.876	9.903	10.044	10.090	**73.63%**
[BTEA]$_2$MnBr$_4$	**9.704**	9.732	9.765	9.957	10.013	10.308	**64.89%**
[TPA]$_2$MnBr$_4$	**9.745**	10.527	10.602	10.637	10.973	11.262	**51.16%**

Table S11. Crystal data and structural refinements for compounds **1**- **4**.

Compound	**1**	**2**	**3**	**4**
chemical formula	$C_{14}N_4H_{26}MnBr_4$	$C_{20}N_2H_{44}MnBr_4$	$C_{24}N_2H_{56}MnBr_4$	$C_{10}N_6H_{28}MnCl_4$
fw	624.97	687.13	747.25	429.12
Space group	$P2_1/c$	$C2/c$	$I2/a$	$P2_1/c$
a/Å	16.0907(13)	32.6167(11)	15.33(8)	12.998(3)
b/Å	9.8057(8)	10.1632(3)	14.54(7)	10.249(2)
c/Å	15.7050(12)	35.3970(13)	31.72(15)	16.616(4)
β/°	110.7980(10)	101.338(7)	96.0(2)	110.645(3)
V(Å^3)	2316.5(3)	11504.8(7)	7032(60)	2070.7(8)
Z	4	16	8	4
D_{calcd} (g·cm^{-3})	1.792	1.471	1.412	1.376
Temp (K)	296.15	293(2)	296.15	269.15
μ (mm^{-1})	7.473	10.277	4.934	1.156
F(000)	1212.0	4736.0	3032.0	892.0
Reflections collected	17432	34526	29013	16348
Unique reflections	2892	11278	5039	2759
Reflections (I>2σ(I))	2213	6092	3439	1998
GOF on F^2	1.005	1.319	1.020	1.048
R_1,wR_2 ($I > 2\sigma(I)$)[a]	0.0292/0.0555	0.1237/0.3467	0.0443/0.1014	0.0607/0.1662
R_1,wR_2 (all data)	0.0480/0.0610	0.1619/0.3883	0.0782/0.1158	0.0868/0.1871
$\Delta\rho_{\text{max}}$ (e/Å^3)	0.44	1.00	0.65	1.01
$\Delta\rho_{\text{min}}$ (e/Å^3)	-0.41	-1.06	-0.55	-0.99

[a] $R_1 = \Sigma||F_o| - |F_c||/\Sigma|F_o|$, $wR_2 = \{\Sigma w[(F_o)^2 - (F_c)^2]^2/\Sigma w[(F_o)^2]^2\}^{1/2}$

Table S12. Crystal data and structural refinements for compounds **5**- **8**.

Compound	**5**	**6**	**7**	**8**
chemical formula	$C_{16}N_4H_{30}MnBr_4$	$C_{14}N_4H_{26}MnCl_4$	$C_{18}N_2H_{28}MnBr_4$	$C_{18}N_2H_{40}MnBr_4$
fw	653.02	447.13	647.00	659.10
Space group	*Pbca*	$P2_1/c$	$P2_1/n$	$P2_1/c$
a/Å	9.44658(14)	16.3551(5)	10.0674(2)	16.2728(7)
b/Å	14.9417(3)	9.3256(2)	18.8439(4)	10.2099(5)
c/Å	34.9546(5)	15.5008(5)	12.9397(3)	17.3145(7)
β/°	90	114.208(4)	94.768(2)	110.204(5)
V(Å^3)	4933.78(14)	2156.30(12)	2459.27(9)	2699.7(2)
Z	8	4	4	4
D_{calcd} (g·cm^{-3})	1.758	1.377	1.747	1.622
Temp (K)	293(2)	293(2)	293(2)	293(2)
μ (mm^{-1})	11.991	9.559	12.128	10.933
F(000)	2552.0	924.0	1260.0	1308.0
Reflections collected	23179	13186	25329	16520
Unique reflections	4963	4230	5047	5250
Reflections (I>2σ(I))	4096	3371	4134	3540
GOF on F^2	1.054	1.058	1.046	1.069
R_1,wR_2 ($I > 2\sigma(I)$)[a]	0.0437/0.1053	0.0804/0.2132	0.0629/0.1648	0.0755/0.1994
R_1,wR_2 (all data)	0.0544/0.1115	0.0967/0.2256	0.0747/0.1727	0.1039/0.2210
$\Delta\rho_{\text{max}}$ (e/Å^3)	0.62	1.45	0.64	0.58
$\Delta\rho_{\text{min}}$ (e/Å^3)	-0.86	-1.04	-1.05	-0.56

[a] $R_1 = \Sigma||F_o| - |F_c||/\Sigma|F_o|$, $wR_2 = \{\Sigma w[(F_o)^2 - (F_c)^2]^2/\Sigma w[(F_o)^2]^2\}^{1/2}$

Table S13. Crystal data and structural refinements for compounds **9**, **10**, **11** and **14**.

Compound	**9**	**10**	**11**	**14**
chemical formula	$C_{26}N_2H_{44}MnBr_4$	$C_{24}N_2H_{56}MnCl_4$	$C_{14}N_2H_{20}MnBr_4$	$C_6N_2H_{16}MnBr_4$
fw	759.21	569.44	590.90	490.76
Space group	*P-1*	*I2/a*	*C2/c*	$P2_1/m$
a/Å	9.7317(2)	14.9953(2)	27.2077(4)	6.3543(8)
b/Å	17.9639(3)	13.8523(2)	8.18571(11)	15.1066(18)
c/Å	18.3238(3)	31.1042(3)	17.9090(3)	7.1756(9)
β/°	81.3050(10)	97.9360(10)	97.9946(13)	90.673(2)
V(Å^3)	3083.52(10)	6399.07(14)	3949.83	688.75(4)
Z	4	8	8	2
D_{calcd} (g·cm^{-3})	1.635	1.182	1.987	2.366
Temp (K)	109.8(2)	293(2)	110.07(11)	296(2)
μ (mm^{-1})	6.674	6.513	10.098	12.531
F(000)	1516.0	2456.0	2264.0	508.0
Reflections collected	43004	17474	14724	4944
Unique reflections	13757	6390	4399	2017
Reflections (I>2σ(I))	13100	5680	4298	1425
GOF on F^2	1.086	1.040	0.998	0.953
R_1,wR_2 (I > 2σ(I))[a]	0.0356/0.0930	0.0451/0.1173	0.0294/0.0811	0.0367/0.0671
R_1,wR_2 (all data)	0.0375/0.0943	0.0515/0.1233	0.0302/0.0818	0.0651/0.0770
$\Delta\rho_{\mathrm{max}}$ (e/Å^3)	1.43	0.38	0.58	0.87
$\Delta\rho_{\mathrm{min}}$ (e/Å^3)	-1.01	-0.56	-1.20	-0.79

[a] $R_1 = \Sigma||F_o| - |F_c||/\Sigma|F_o|$, $wR_2 = \{\Sigma w[(F_o)^2 - (F_c)^2]^2/\Sigma w[(F_o)^2]^2\}^{1/2}$

References:

1 L. J. Xu, C. Z. Sun, H. Xiao, Y. Wu and Z. N. Chen, *Adv. Mater.*, 2017, **29**, 1605739.

2 L. L. Mao, P. J. Guo, S. X. Wang and A. K. Cheetham, *J. Am. Chem. Soc.*, 2020, **142**, 13582-13589.

3 L. J. Xu, X. S. Lin, Q. Q. He, M. Worku and B. W. Ma, *Nat. Commun.*, 2020, **11**, 4329.

4 Z. X. Wang, P. F. Li, W. Q. Liao, Y. Y. Tang, H. Y. Ye and Y. Zhang, *Chem. Asian. J.,* 2016, **11**, 981 985.

5 S. Q. Chen, J. M. Gao, J. Y. Chang, Y. Zhang and L. Feng, *Sensor. Actuat. B-Chem.,* 2019, **297**, 126701.

6 G. j. Zhou, Z. Y. Liu, J. L. Huang, M. S. Molokeev, Z. W. Xiao, C. G. Ma and Z. G. Xia, *J. Phys. Chem. Lett.,* 2020, **11**, 5956–5962.

7 H. M. Fu, C. L. Jiang, J. Lao, C. H. Luo, H. C. Lin, H. Peng and C. G. Duan, *CrystEngComm.,* 2020, **22**, 1436-1441.

8 L.-K. Gong, Q.-Q. Hu, F.-Q. Huang, Z.-Z. Zhang, N.-N. Shen, B. Hu, Y. Song, Z.-P. Wang, K.-Z. Du and X.-Y. Huang, *Chem. Commun.,* 2019, **55**, 7303-7306.

9 M.-Z. Li, J. Zhou, M. S. Molokeev, X.-X. Jiang, Z. S. Lin, J. Zhao and Z.-G. Xia, *Inorg. Chem.,* 2019, **58**, 13464-13470.

10 Y. L. Wei, J. Jing, C. Shi, H. Y. Ye, Z. X. Wang and Y. Zhang, *Inorg. Chem. Front.,* 2018, **5**, 2615-2619.

11 V. Morad, I. Cherniukh, L. Pöttschacher, Y. Shynkarenko, S. Yakunin and M. V. Kovalenko, *Chem. Mater.,* 2019, **31**, 10161-10169.

12 X. W. Cai, Y. Y. Zhao, H. Li, C. P. Huang and Z. Zhou, *J. Mol. Struct.,* 2018, **1161**, 262-266.

13 Y. D. Deng, X. H. Dong, M. Yang, H. M. Zeng, G. H. Zou and Z. E. Lin, *Dalton Trans.,* 2019, **48**, 17451-17455.

14 C. L. Jiang, N. Zhong, C. H. Luo, H. C. Lin, Y. Y. Zhang, H. Peng and C. G. Duan, *Chem. Commun.,* 2017, **53**, 5954-5957.

15 Y. Y. Luo, Z. X. Zhang, C. Y. Su, W. Y. Zhang, P. P. Shi, Q. Ye and D. W. Fu, *J. Mater. Chem. C,* 2020, **8**, 7089-7095.

16 Y X. Wu, C. F. Wang, H. H. Li, F. Jiang, C. Shi, H. Y. Ye and Y. Zhang, *Eur. J. Inorg. Chem.,* 2020, **2020**, 394-399.

17 B. B. Su, M. S. Molokeeva and Z. G. Xia, *J. Mater. Chem. C,* 2019, **7**, 11220-11226.

18 C. Zhou, H. Lin, J. Neu, Y. Zhou, M. Chaaban, S. Lee, M. Worku, B. Chen, R. Clark, W. Cheng, J. Guan, P. Djurovich, D. Zhang, X. Lü, J. Bullock, C. Pak, M. Shatruk, M.-H. Du, T. Siegrist and B. Ma, *ACS Energy Lett.*, 2019, **4**, 1579-1583.

19 M. Li, Y. Li, M. S. Molokeev, J. Zhao, G. Na, L. Zhang and Z. Xia, *Adv. Opt. Mater.*, 2020, **8**, 2000418

20 M. Li, J. Zhou, G. Zhou, M. S. Molokeev, J. Zhao, V. Morad, M. V. Kovalenko and Z. Xia, *Angew. Chem. In.t Ed.*, 2019, **58**, 18670-18675.

21 J. Zhou, M. Li, L. Ning, R. Zhang, M. S. Molokeev, J. Zhao, S. Yang, K. Han and Z. Xia, *J. Phys. Chem. Lett.*, 2019, **10**, 1337-1341.

22 Q. Li, Z. Chen, M. Li, B. Xu, J. Han, Z. Luo, L. Tan, Z. Xia and Z. Quan, *Angew. Chem. Int. Ed.*, 2021, **60**, 2583-2587.

23 T. Ahmed, S. Seth and A. Samanta, *Chem. Mater.*, 2018, **30**, 3633-3637.

24 T. Zhao, H. Liu, M. E. Ziffer, A. Rajagopal, L. Zuo, D. S. Ginger, X. Li and A. K. Y. Jen, *ACS*

Energy Lett., 2018, **3**, 1662-1669.

25 D. Yu, F. Cao, Y. Gao, Y. Xiong and H. Zeng, *Adv. Funct. Mater.*, 2018, **28**. 1800248

26 S. Kumar, J. Jagielski, N. Kallikounis, Y. H. Kim, C. Wolf, F. Jenny, T. Tian, C. J. Hofer, Y. C. Chiu, W. J. Stark, T. W. Lee and C. J. Shih, *Nano. Lett.*, 2017, **17**, 5277-5284.

27 P. Sebastia-Luna, J. Navarro-Alapont, M. Sessolo, F. Palazon and H. J. Bolink, *Chem. Mater.*, 2019, **31**, 10205-10210.

28 S. Li, L. Wang, D. Tang, Y. Cho, X. Liu, X. Zhou, L. Lu, L. Zhang, T. Takeda, N. Hirosaki and R.-J. Xie, *Chem. Mater.*, 2017, **30**, 494-505.

29 E. H. Song, Y. Y. Zhou, Y. Wei, X. X. Han, Z. R. Tao, R. L. Qiu, Z. G. Xia and Q. Y. Zhang, *J. Mater. Chem. C*, 2019, **7**, 8192-8198.

30 Y. Zhu, Y. Liang, S. Liu, H. Li and J. Chen, *Advanced Optical Materials*, 2019, **7**, 1801419.

31 P. Strobel, S. Schmiechen, M. Siegert, A. Tücks, P. J. Schmidt and W. Schnick, *Chem. Mater.*, 2015, **27**, 6109-6115.

32 T. Takeda, N. Hirosaki, S. Funahshi, R. J. Xie, *Chem. Mater*., 2015, **27**, 5892-5898.

33 M. Zhao, H. Liao, L. Ning, Q. Zhang, Q. Liu and Z. Xia, *Adv. Mate.r*, 2018, **30**, 1802489.

34 J. S. Lee, S. Unithrattil, S. Kim, I. J. Lee, H. Lee and W. B. Im, *Opt. Lett.*, 2013, **38**, 3298-3300.